Fall 2025 ULAB Physics & Astronomy Project Proposal Presentations

Abby’s Group

Analyzing Gas Structure of Galaxy-Clusters via Multipole Decomposition

Finding Dominant Multipole Moments With χ^2 Analysis

Theo Barbou-des-Places, Anirudh Kumaraswamy, Minh Le, Bruno Leopoldo, Jonathan Pan, Jeevika Rajasekar

Mentor: Abby Schleigh

Background

- Galaxy Clusters
  - Galaxies, baryonic gas, dark matter

- Incomplete understanding of gas structure in galaxy clusters

Credit: NASA, ESA, and J. Lotz and the HFF Team (STScI)

Background

- kSZ (kinematic Sunyaev-Zeldovich) Effect
  - Photons interact with electrons with high kinetic energies

$$\frac{\delta T_{kSZ}(\hat{n})}{T_{CMB}} = -\int \frac{d\chi}{1+z} n_e(\chi\hat{n}, z)\sigma_T e^{-\tau(z)} \frac{\nu_{\mathbf{e}} \cdot \hat{\mathbf{n}}}{c}$$

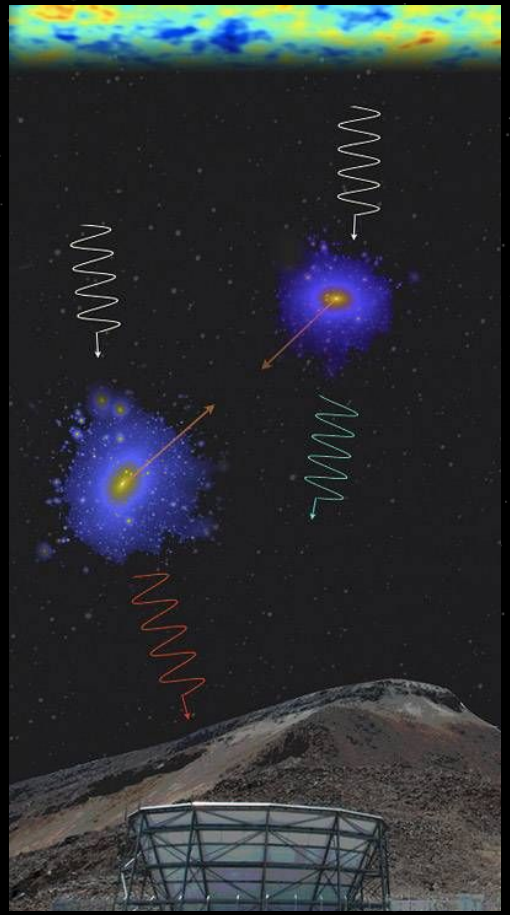

kSZ effect

(Image by Sudeep Das, University of California-Berkeley)

Background

- tSZ (thermal Sunyaev-Zeldovich) Effect
  - Photons interact with electrons with high thermal energy
  - Inverse Compton Scattering

$$y = \int n_e \frac{k_B T_e}{m_e c^2} \sigma_T dl$$

$$\frac{\Delta T}{T_{CMB}} = y(x\frac{e^x + 1}{e^x - 1} - 4)$$

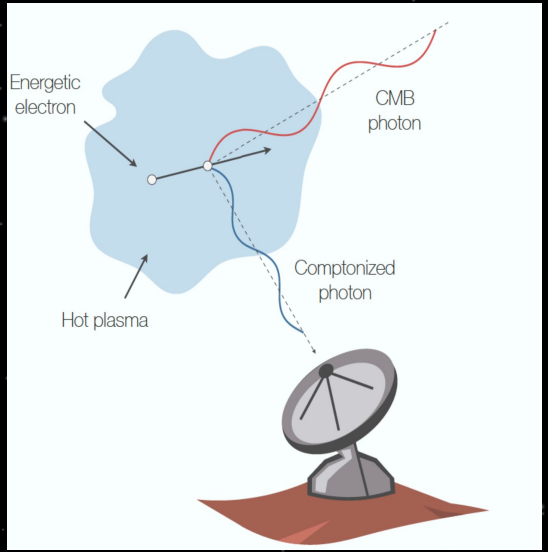

tSZ effect

Background

- Lensing profile (Kappa map)
  - SZ profiles mainly consider baryonic matter (i.e. “normal” matter)
  - Kappa includes dark matter and offers a reference to validate the data

$$\kappa(\theta) = \int \frac{l dl}{2\pi} J_0(l\theta) C_l^{g\kappa}$$

Background

- Multipole Decomposition
  - Profiles can decomposed into multipoles
  - Each multipole represents a different level of complexity of the cluster's structure
  - m = 0 represents the simplest level, and higher values represent increasingly complex aspects of the structure

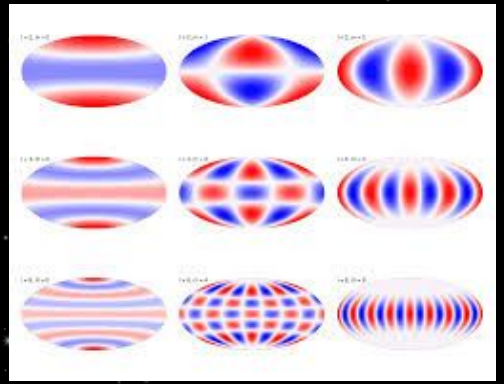

Research Question

We will construct kSZ and tSZ mean profiles from the ACT DR5 Cluster-SZ catalog, and we will perform multipole decomposition of those profiles. Through $\square^2$ analysis, we will determine which multipole is “dominant” for each original profile, which will allow us a greater understanding of the structure of baryonic gas in galaxy clusters.

Analysis of Gas Structure (Methods)

How is baryonic matter detected throughout clusters?

- The ACT telescope outputs signal maps (tSZ, kSZ, lensing convergence).
- The respective profiles of SZ signals, and kappa maps from the CMB

Atacama Cosmology Telescope (ACT)

Lensing Convergence Map

$$\kappa(\theta) = \int \frac{l dl}{2\pi} J_0(l\theta) C_l^{g\kappa}$$

- For given cluster samples, we replicate Hadzhiyska's methods in a Fourier transform of the cluster-matter power spectrum to a continuous map κ.
- This is a general calculation of the map for lensing convergence throughout clusters.

tSZ Signal Map

- The Compton-y parameter is a parameterization of the tSZ effect
- We need to construct our tSZ signal map, as seen below the Compton-y

$$y \equiv \sigma_T \int dl \; n_e \frac{k(T_e - T_{\mathrm{CMB}})}{m_e c^2}$$

$$\frac{\Delta T}{T_{\mathrm{CMB}}} = y \left(x \frac{e^x + 1}{e^x - 1} - 4 \right)$$

$$x = \frac{h\nu}{k_B T_{CMB}}$$

ThumbStack - CAP filter

- Python Package
- Removes noise (small fluctuations in the CMB)
- Acts as a band pass filter
- Same for tSZ and kSZ
- Creates a disk with radius θ_d and ring of same area around disk, calculates mean signal of both, subtracts signal of ring from disk

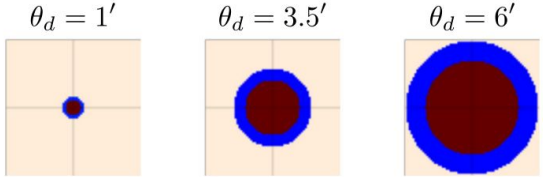

$$T(\theta_d) = \int d^2\theta \delta T(\theta) \qquad W_{\theta_d}(\theta) = \begin{cases} 1 & \text{for } \theta < \theta_d, \\ -1 & \text{for } \theta_d \leq \theta \leq \sqrt{2}\theta_d, \\ 0 & \text{otherwise.} \end{cases}$$

ThumbStack - tSZ Stacking

- After the tSZ profiles for every cluster has been created, we need to stack them to make mean profiles
- Removes noise
- Improves signal strength
- To do this, we take the inverse variance weighted mean

$$\hat{T}_{\mathrm{tSZ}}(\theta_d) = \frac{\sum_i \mathcal{T}_i(\theta_d)/\sigma_i^2}{\sum_i 1/\sigma_i^2},$$

ThumbStack - kSZ Stacking

- Velocity-weighted, inverse-variance weighted mean
- Solve linear continuity equation with cluster overdensity to get 3D velocity field
- Based on the galaxy linear bias
- Only line of sight component is needed

$$\delta_g = b\delta_{m'}$$

$$\nabla \cdot \boldsymbol{v} + f\nabla \cdot [(\boldsymbol{v} \cdot \hat{\boldsymbol{n}})\hat{\boldsymbol{n}}] = -aHf\frac{\delta_g}{b}.$$

$$\hat{T}_{kSZ}(\theta_d) = -\frac{1}{r_\nu}\frac{v_{rms}^{rec}}{c}\frac{\sum_i T_i(\theta_d)(v_{rec,i}/c)/\sigma_i^2}{\sum_i (v_{rec,i}/c)^2/\sigma_i^2}$$

Signal Stacking & Multipole Decomposition

- Extract square cutouts of angular patches of the sky
- Model all 3 fields: kSZ, tSZ, gravitational lensing
- Compute observed field
- Average reprojected profile
- Construct decomposed profile at each multipole

$$F_{\mathrm{tot}}(\theta) = \sum_{i=1}^{N} F_i(\theta)$$

$$\overline{F}(r_k) = \frac{1}{N_k} \sum_{\theta_j \in A_k} \overline{F}(\theta_j)$$

$$F_m(r) = \frac{1}{2\pi} \int_0^{2\pi} \overline{F}(r,\theta)\, e^{-im\theta}\, d\theta$$

Multipole profiles

- Anisotropic properties
- m = 0, m = 1, m = 2, ...
- Properties and gas distribution
- Dominant multipole m =1 (merging of clusters)

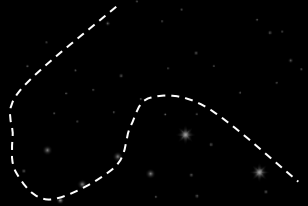

$$F_1(r)e^{i\theta} + F_{-1}(r)e^{-i\theta} \sim A(r)\cos\theta + B(r)\sin\theta.$$

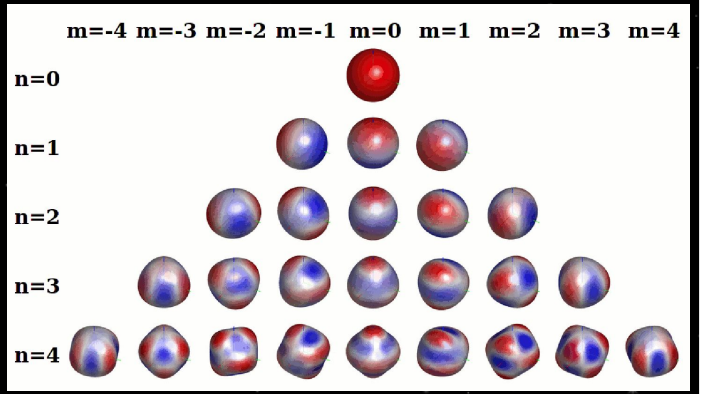

χ^2 (chi^2) Analysis pt 1

- What are we doing with all these profiles, decompositions?
- Compare each multipole moment with the original profile
  - Calculate cross covariance matrix
- $p_i = F_m(r)$, 1d array for multipole moment
- Similarly, $p_j = F_o(r)$, original profile

$$
\begin{aligned}
\mathrm{C}_{ii} &= \langle (p_i - \bar{p}_i)(p_i - \bar{p}_i)^T \rangle \\
\mathrm{C}_{jj} &= \langle (p_j - \bar{p}_j)(p_j - \bar{p}_j)^T \rangle \\
\mathrm{C}_{ij} &= \langle (p_i - \bar{p}_i)(p_j - \bar{p}_j)^T \rangle \\
\mathrm{C} &= \mathrm{C}_{ii} + C_{jj} - C_{ij} - C_{ji}
\end{aligned}
$$

$$
\chi^2 \equiv (p_i - p_j) \cdot (C)^{-1} \cdot (p_i - p_j)
$$

χ^2 (chi^2) Analysis pt 2

- Data validation
  - To check for dust, use: $$\chi^2_m(r) = \frac{\left| F_m^{\text{obs}}(r) - F_m^{\text{model}}(r) \right|^2}{\sigma_m(r)^2}.$$ with ML for F^{model}
  - To check for dark matter, compare to lensing profile
  - To check for merging, check χ^2 for m = 1

Timeline

1/12–1/25:

- Download necessary catalogs, maps, and masks
- Getting our packages via python to work

1/26–2/08:

- begin work on original radial profiles
- plugging our maps and cluster SZ data into ThumbStack.

2/09–2/22:

- finish up the radial profiles and calculate the mean profiles
- being figuring out how multipole decomposition on kSZ works.

2/23–3/07:

- begin decomposing original profiles into multipoles.

Timeline

3/08–3/21:

- Continue focus on the multipole decomposition of the profiles, considering how much information we can extract through this process

3/22–4/04:

- Run chi-squared tests between different sets of our data
- Compare the decompositions to the original profiles
- Compare different types of profiles to each other (e.g. tSZ and kSZ)

4/05–4/18:

- buffer period (in case we're behind in a previous step)
- begin drafting our final project poster and presentation.

Expenses/Resources

- No expenses are anticipated, as all necessary data is publicly available through ACT.

References

[1] B. Hadzhiyska et al., arXiv preprint arXiv:2507.14136 (2025).
[2] M. Lokken et al., The Astrophysical Journal 982, 186 (2025).
[3] E. Schaan et al., Physical Review D 103, 063513 (2021).
[4] M. Hilton et al., The Astrophysical Journal Supplement Series 253, 3 (2021).
[5] M. Lokken et al., The Astrophysical Journal 933, 134 (2022).
[6] Z. Huang, Physical Review D 93, 043538 (2016).
[7] N. Aghanim, S. Majumdar, and J. Silk, Reports on Progress in Physics 71, 066902 (2008).
[8] R. Sunyaev and Y. B. Zeldovich, Comments on Astrophysics and Space Physics, Vol. 4,
p. 173 4, 173 (1972).

Aidan’s Group

Quantifying Stripping in the Hydrogen Rich Supernova SN 2023axu

Mentees:
Isaac Chan
Alberto Diaz
Anirvan Gautam
Jeankarlo Gonzalez
Sai Praneth K.
Rianna Marquez

Mentor:
Aidan Martas

Overview

- **Goal**: Studying SN 2023axu (typical Type IIP supernova) spectroscopic and photometric data
  - Photometric data reduced with the lcogtsnpipe pipeline

- Analyze SN 2023axu through radiative hydrodynamic modeling (RHD)
  - Determine progenitor metrics
- Growth in sample size of partially stripped Type IIP SN progenitors has led to motivation to investigate envelope stripping

Image credits: © pongpinun/Stock.adobe.com

Core Collapse Supernovae (CCSNe)

- Explosions of stars $\gtrsim 8 M_\odot$
  - Can be Type II, Type Ib or Type Ic
  - Provide crucial information about progenitors such as:
    - Type of heavy elements produced
    - Stellar environment prior to explosion
  - Photometry can provide insight to presence of circumstellar material (CSM), progenitor metrics, and ^{56}Ni mass
- Nucleosynthesis of CCSN progenitors:
  - Fuse up to iron in core
- CCSN explosion
  - Fuses heavier elements, with one of the products ^{56}Ni powering the nebular tail of the light curve through radioactive decay
  - Elements like Ca, Mg, etc. become more prominent in the spectra as temperature decreases and the supernova becomes more optically thin

Image credits: https://science.nasa.gov/photojournal/kepler-beyond-planets-finding-exploding-stars-core-collapse-supernova/

Type II (Hydrogen-Rich Core-Collapse) Supernovae

- Most frequently observed core collapse supernova
- Prominent hydrogen lines in their spectra
- Photometry, Spectra vary greatly depending on subclasses
  - Subclasses include: IIL, IIn, IIb
  - Differences linked to progenitor parameters
- Circumstellar Material (CSM) presence
  - One of the key properties for all Type II progenitors
  - May interact with supernova ejecta
    - Increase in luminosity at the start of the system
    - Alters hydrogen emission line geometry

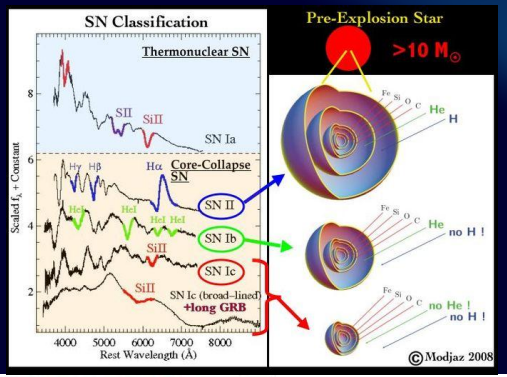

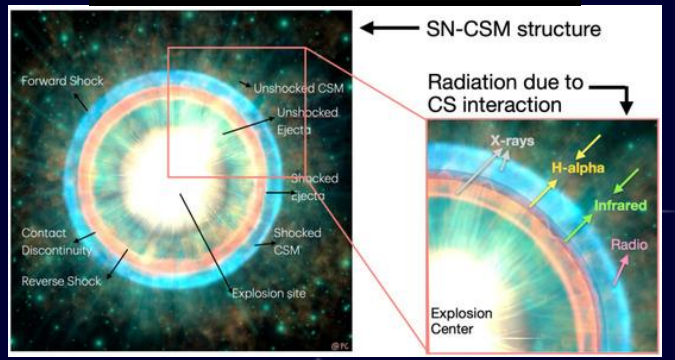

Image credits (top to bottom): M. Modjaz https://www.mdpi.com/2218-1997/11/11/363, Poonam Chandra https://doi.org/10.3390/universe11110363

Type II Plateau (IIP) Supernovae

- Result from the explosion of red supergiants
- Display an extended plateau in luminosity lasting ~100 days
  - Evolution of the hydrogen recombination boundary is responsible
- Plateau ends when hydrogen sustaining the boundary is depleted
  - Ejecta becomes optically thin
- Plateau phase followed by nebular phase
  - Linear decline in luminosity powered by Ni decay chain
  - $^{56}Ni \rightarrow {}^{56}Co \rightarrow {}^{56}Fe$

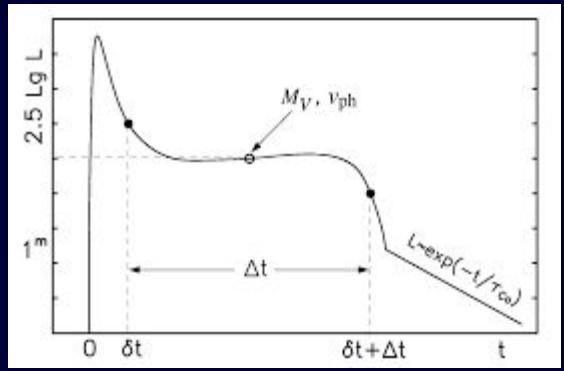

Image credits: Elisabeth Gall et. al https://www.eso.org/~bleibund/talks/Bonn16-EPM-pub.pdf

Motivation

- The Theory:
  - Type SNe IIP defined light curve plateau
  - More Progenitor Mass → More Hydrogen (H) → Longer plateau

- The Contradiction:
  - Recent survey (Das et al. 2025) weak correlation (r = 0.42) between brightness & plateau duration
  - High mass stars are exploding with short plateaus

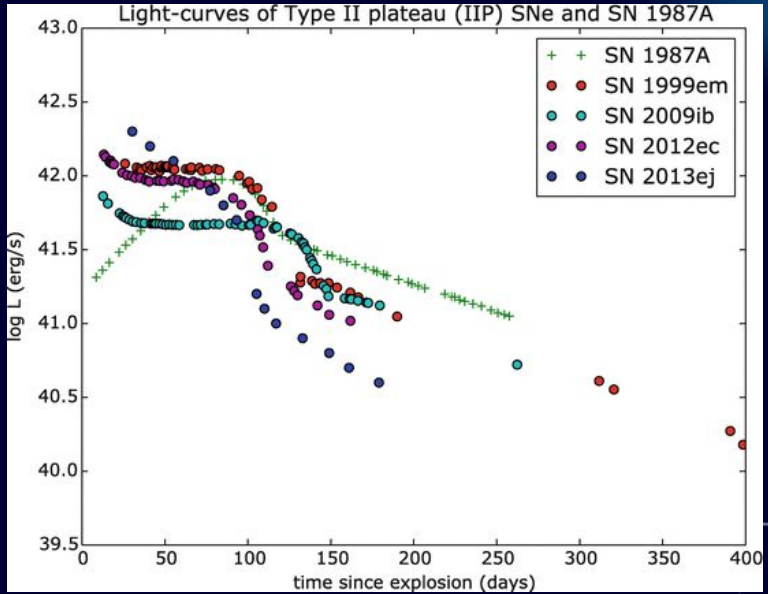

Research Question

- The Hypothesis:
  - **Envelope Stripping**: removal of H in progenitor
  - Likely caused by binary interactions or stellar winds
- Precedent Studies:
  - Analyses of SN2023ixf & SN2019hnl showed “partial stripping” models required to fit the photometry
- Our objective:
  - Perform similar RHD analysis on a new target: SN2023axu

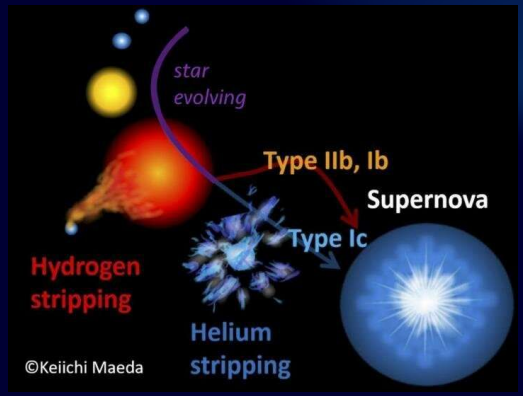

Partial stripping

- Causes lighter hydrogen envelopes
  - Less hydrogen → shorter plateau phase
- Concentration of Ni-56 emitting high energy gamma rays → more heat → extends the plateau
- Theories in red supergiants
  - Episodic mass loss (Stellar pulsations)
    - Quick CSM movement
  - Superwinds
  - Binary star interaction

Binary star interaction

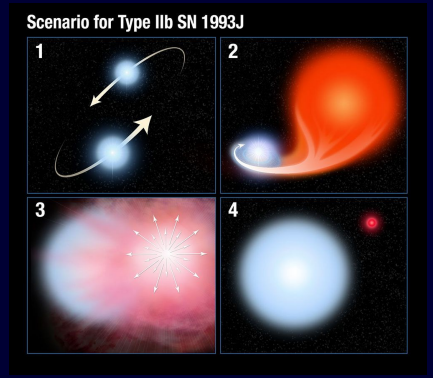

Superwinds

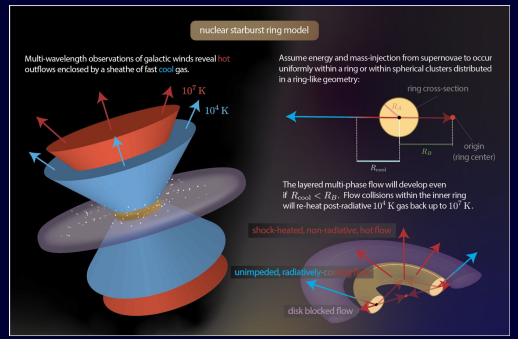

Partial stripping

- Causes lighter hydrogen envelopes
  - Less hydrogen → shorter plateau phase
- Ni-56 extends plateau from gamma-ray reprocessing
- Theories in red supergiants
  - Episodic mass loss (Stellar pulsations)
  - Superwinds
  - Binary star interaction

Episodic mass loss

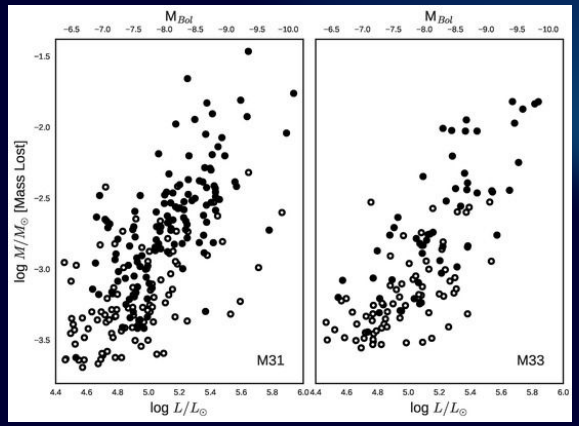

Binary star interaction

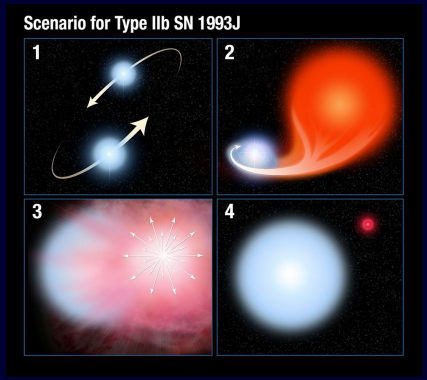

Superwinds

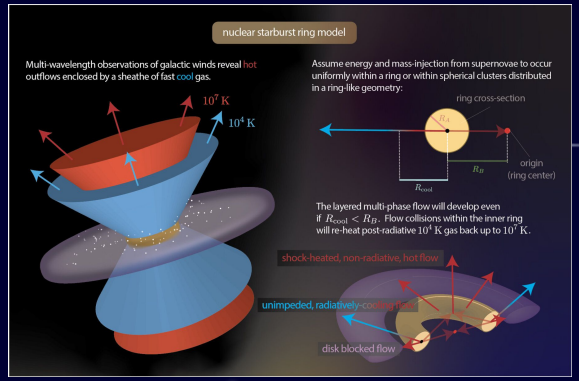

Photometry reduction

- Obtained multi-band imaging of SN 2023axu from **LCO (gri)** and **DLT40 (B, V, g, r, i)** to build a broad optical dataset.
- Processed LCO observations using the **lcogtsnpipe pipeline** to perform image subtraction, photometric calibration, and point-source extraction.
- Combined LCO and DLT40 photometry into a unified dataset for consistent light-curve construction.
- Corrected all observations for **Milky Way extinction** to produce an initial **dereddened light curve**.
- Plan to apply an additional **host-galaxy extinction correction** next semester.

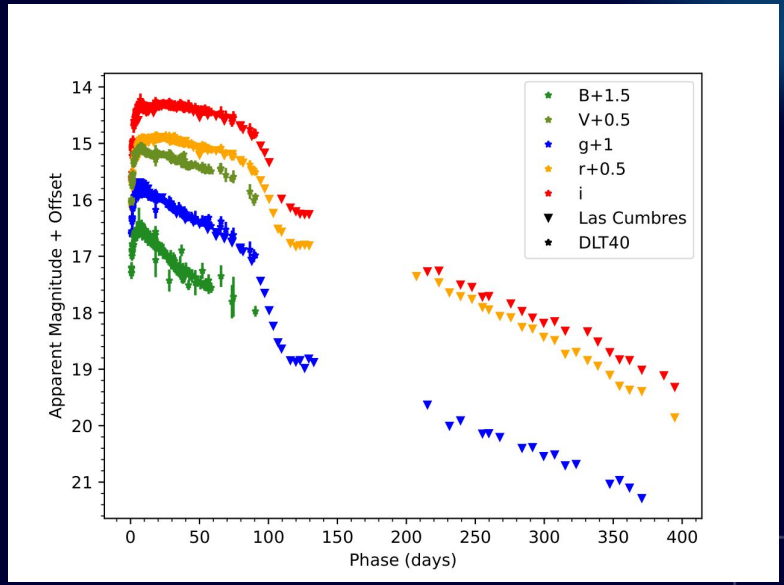

Radiative Hydrodynamic Modeling

- Plan to use RHD to generate models of stellar evolution and supernovae light curves
- Fit those models to observations of SN2023axu to find the most likely model
- MESA (Stellar Evolution)
  - Model the stellar evolution of the progenitor star of SN2023axu
  - Progenitor mass, explosion energy, and ^{56}Ni mass
  - Parameters for an artificially scaled stellar wind to model partial stripping
- STELLA (Supernova)
  - Synthesize the light curve of the progenitor star modeled by MESA after shock breakout
  - Model CSM as a mass-loss element due to stellar wind

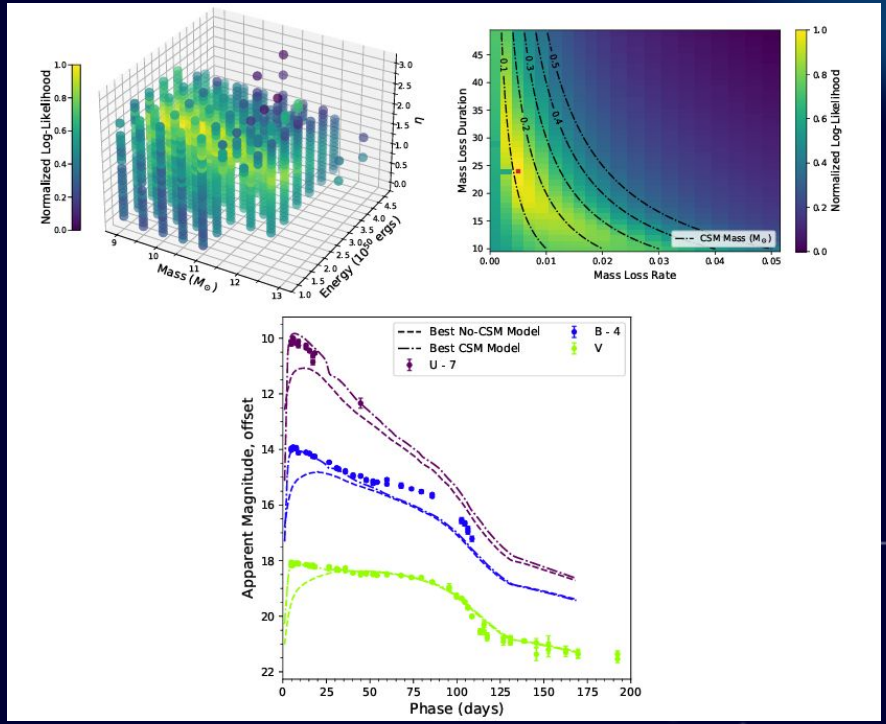

Image credits: Martas et al. (2025)

Spectral analysis

- Plan to compare SN 2023axu's spectra to a set of well-studied SNe II-P to establish a baseline for normal behavior.
- Look at the evolution of hydrogen features (specifically Hα) to check for signs of weakened hydrogen emission at nebular times.
- Use the [O I] λ6300, λ6364 doublet to estimate the progenitor's core mass.
- Compare the expected Hα strength (based on core mass) with what we observe to test for possible hydrogen stripping.
- Use these comparisons as an initial observational check for signs of envelope loss.

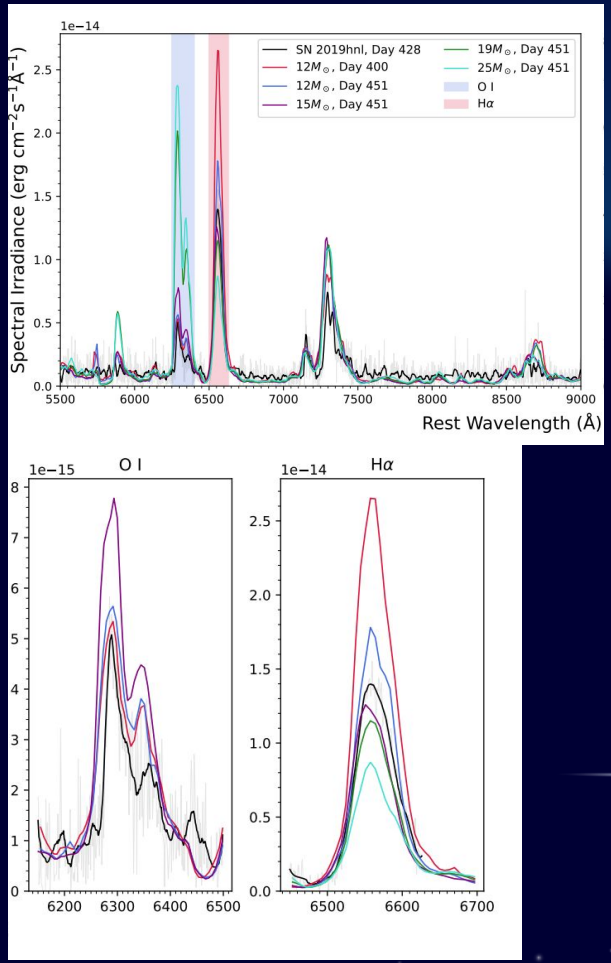

Image credits: Martas et al. (2025)

Expenses and Resources

- O(10^2) - O(10^3) RHD models
- A single model requires ~ 10^3 s of CPU time across 32 threads of an AMD Ryzen 9 7950X processor
- Compute server (i.e. Savio) will be needed to run in a realistic timeframe

Timeline

- 01/19-01/26: Complete data dereddening & measure Ni-56 mass in preparation for RHD modeling
- 01/26-02/02: Finalize Ni-56 mass calculations, measure spectral and photometric statistics to compare with other SNe II
- 02/02-02/09: Finalize spectral statistics, compare spectra with RHD models
- 02/09-02/16: Begin RHD modeling with MESA+STELLA
- 02/16-02/23: Run, debug MESA+STELLA models
    - Repeat weekly 02/23-03/16
- 03/16-03/23: Continue analysis of MESA+STELLA models, finalizing results
- 03/23-03/30: Draw conclusions from MESA+STELLA models, determine if spectral modeling is justified
- 03/30-04/06: Compare results to that of similar SNe, identify connections and similarities in derived quantities
- 04/06-04/13: Buffer week for spectral modeling if chosen
    - Repeat weekly 04/13-04/20
- 04/20-04/27: Begin writing up project presentation
- 04/27-05/04: Finish writing up project presentation
- 05/04-05/08: Presentation

Timeline

- 01/19-01/26: Complete data dereddening & measure Ni-56 mass in preparation for RHD modeling
- 01/26-02/02: Finalize Ni-56 mass calculations, measure spectral and photometric statistics to compare with other SNe II
- 02/02-02/09: Finalize spectral statistics, compare spectra with RHD models
- 02/09-02/16: Begin RHD modeling with MESA+STELLA
- 02/16-02/23: Run, debug MESA+STELLA models
    - Repeat weekly 02/23-03/16
- 03/16-03/23: Continue analysis of MESA+STELLA models, finalizing results
- 03/23-03/30: Draw conclusions from MESA+STELLA models, determine if spectral modeling is justified
- 03/30-04/06: Compare results to that of similar SNe, identify connections and similarities in derived quantities
- 04/06-04/13: Buffer week for spectral modeling if chosen
    - Repeat weekly 04/13-04/20
- 04/20-04/27: Begin writing up project presentation
- 04/27-05/04: Finish writing up project presentation
- 05/04-05/08: Presentation

Works Cited

Chandra, Poonam. 2025. "Multiwavelength View of Circumstellar Interaction in Supernovae" *Universe* 11, no. 11: 363. https://doi.org/10.3390/universe11110363

References

Blinnikov, S., Lundqvist, P., Bartunov, O., Nomoto, K., and Iwamoto, K. (2000). Radiation hydrodynamics of sn 1987a. i. global analysis of the light curve for the first 4 months. *The Astrophysical Journal*, 532(2):1132.

Blinnikov, S., Röpke, F., Sorokina, E. I., Gieseler, M., Reinecke, M., Travaglio, C., Hillebrandt, W., and Stritzinger, M. (2006). Theoretical light curves for deflagration models of type ia supernova. *Astronomy & Astrophysics*, 453(1):229–240.

Blinnikov, S. I., Eastman, R., Bartunov, O. S., Popolitov, V. A., and Woosley, S. E. (1998). A Comparative Modeling of Supernova 1993J. , 496(1):454–472.

Branch, D. and Wheeler, J. C. (2017). *Spectra*, pages 47–74. Springer Berlin Heidelberg, Berlin, Heidelberg.

Das, K. K., Kasliwal, M. M., Sollerman, J., Fremling, C., Moriya, T. J., Hinds, K.-R., Perley, D. A., Bellm, E. C., Chen, T. X., O'Connor, E. P., Coughlin, M. W., Jacobson-Galan, W. V., Gangopadhyay, A., Graham, M., Kulkarni, S. R., Purdum, J., Sarin, N., Schulze, S., Singh, A., Tsuna, D., and Wold, A.

(2025). Low-Luminosity Type IIP Supernovae from the Zwicky Transient Facility Census of the Local Universe. II: Lightcurve Analysis. *arXiv e-prints*, page arXiv:2506.20068.

Fang, Q., Moriya, T. J., Ferrari, L., Maeda, K., Folatelli, G., Ertini, K. Y., Kuncarayakti, H., Andrews, J. E., and Matsumoto, T. (2024). Diversity in hydrogen-rich envelope mass of type ii supernovae. ii. sn 2023ixf as explosion of partially stripped intermediate massive star. *The Astrophysical Journal*, 978(1):36.

Gräfener, G. and Vink, J. S. (2015). Light-travel-time diagnostics in early supernova spectra: substantial mass-loss of the iib progenitor of sn 2013cu through a superwind. *Monthly Notices of the Royal Astronomical Society*, 455(1):112–126.

Jerkstrand, A., Smartt, S. J., Fraser, M., Fransson, C., Sollerman, J., Taddia, F., and Kotak, R. (2014). The nebular spectra of sn 2012aw and constraints on stellar nucleosynthesis from oxygen emission lines. *Monthly Notices of the Royal Astronomical Society*, 439(4):3694–3703.

Jermyn, A. S., Bauer, E. B., Schwab, J., Farmer, R., Ball, W. H., Bellinger, E. P., Dotter, A., Joyce, M., Marchant, P., Mombarg, J. S. G., Wolf, W. M., Sunny Wong, T. L., Cinquegrana, G. C., Farrell, E., Smolec, R., Thoul, A., Cantiello, M., Herwig, F., Toloza, O., Bildsten, L., Townsend, R. H. D., and Timmes, F. X. (2023). Modules for Experiments in Stellar Astrophysics (MESA): Time-dependent Convection, Energy Conservation, Automatic Differentiation, and Infrastructure. , 265(1):15.

Ma, J.-Z., Justham, S., Pakmor, R., Chiavassa, A., Ryu, T., and de Mink, S. (2025). AREPO-RSG: Aspherical Circumstellar Material and Winds from Pulsating Dusty Red Supergiants in Global 3D Radiation Hydrodynamic Simulations. *arXiv e-prints*, page arXiv:2510.14875.

Martas, A., Valenti, S., Ravi, A. P., Dong, Y., Bostroem, K. A., Pearson, J., Shrestha, M., Andrews, J. E., Sand, D. J., Hosseinzadeh, G., Lundquist, M., Hoang, E., Mehta, D., Meza Retamal, N., Jha, S. W., Janzen, D., Howell, D. A., McCully, C., Hiramatsu, D., and Pellegrino, C. (2025). Sn 2019hnl: A type iip supernova with a partially stripped, low-mass progenitor. *The Astrophysical Journal*, 993(1):28.

Paxton, B., Bildsten, L., Dotter, A., Herwig, F., Lesaffre, P., and Timmes, F. (2011). Modules for Experiments in Stellar Astrophysics (MESA). , 192(1):3.

Paxton, B., Cantiello, M., Arras, P., Bildsten, L., Brown, E. F., Dotter, A., Mankovich, C., Montgomery, M. H., Stello, D., Timmes, F. X., and Townsend, R. (2013). Modules for Experiments in Stellar Astrophysics (MESA): Planets, Oscillations, Rotation, and Massive Stars. , 208(1):4.

Paxton, B., Marchant, P., Schwab, J., Bauer, E. B., Bildsten, L., Cantiello, M., Dessart, L., Farmer, R., Hu, H., Langer, N., Townsend, R. H. D., Townsley, D. M., and Timmes, F. X. (2015). Modules for Experiments in Stellar Astrophysics (MESA): Binaries, Pulsations, and Explosions. , 220(1):15.

Paxton, B., Schwab, J., Bauer, E. B., Bildsten, L., Blinnikov, S., Duffell, P., Farmer, R., Goldberg, J. A., Marchant, P., Sorokina, E., Thoul, A., Townsend, R. H. D., and Timmes, F. X. (2018). Modules for Experiments in Stellar Astrophysics (MESA): Convective Boundaries, Element Diffusion, and Massive Star Explosions. , 234(2):34.

Paxton, B., Smolec, R., Schwab, J., Gautschy, A., Bildsten, L., Cantiello, M., Dotter, A., Farmer, R., Goldberg, J. A., Jermyn, A. S., Kanbur, S. M., Marchant, P., Thoul, A., Townsend, R. H. D., Wolf, W. M., Zhang, M., and Timmes, F. X. (2019). Modules for Experiments in Stellar Astrophysics (MESA): Pulsating Variable Stars, Rotation, Convective Boundaries, and Energy Conservation. , 243(1):10.

Shrestha, M., Pearson, J., Wyatt, S., Sand, D. J., Hosseinzadeh, G., Bostroem, K. A., Andrews, J. E., Dong, Y., Hoang, E., Janzen, D., Jencson, J. E., Lundquist, M., Mehta, D., Retamal, N. M., Valenti, S., Rastinejad, J. C., Daly, P., Porter, D., Hinz, J., Self, S., Weiner, B., Williams, G. G., Hiramatsu, D., Howell, D. A., McCully, C., Gonzalez, E. P., Pellegrino, C., Terreran, G., Newsome, M., Farah, J., Itagaki, K., Jha, S. W., Kwok, L., Smith, N., Schwab, M., Rho, J., and Yang, Y. (2024). Evidence of weak circumstellar medium interaction in the type ii sn 2023axu. *The Astrophysical Journal*, 961(2):247.

Tartaglia, L., Sand, D. J., Valenti, S., Wyatt, S., Anderson, J. P., Arcavi, I., Ashall, C., Botticella, M. T., Cartier, R., Chen, T.-W., Cikota, A., Coulter, D., Della Valle, M., Foley, R. J., Gal-Yam, A., Galbany,

L., Gall, C., Haislip, J. B., Harmanen, J., Hosseinzadeh, G., Howell, D. A., Hsiao, E. Y., Inserra, C., Jha, S. W., Kankare, E., Kilpatrick, C. D., Kouprianov, V. V., Kuncarayakti, H., Maccarone, T. J., Maguire, K., Mattila, S., Mazzali, P. A., McCully, C., Melandri, A., Morrell, N., Phillips, M. M., Pignata, G., Piro, A. L., Prentice, S., Reichart, D. E., Rojas-Bravo, C., Smartt, S. J., Smith, K. W., Sollerman, J., Stritzinger, M. D., Sullivan, M., Taddia, F., and Young, D. R. (2018). The Early Detection and Follow-up of the Highly Obscured Type II Supernova 2016ija/DLT16am. , 853(1):62.

Valenti, S. (2016). The diversity of type ii supernova versus the similarity in their progenitors. *arXiv preprint*.

Vartanyan, D., Laplace, E., Renzo, M., Götberg, Y., Burrows, A., and de Mink, S. E. (2021). Binary-stripped stars as core-collapse supernovae progenitors. *The Astrophysical Journal Letters*, 916(1):L5.

Thank you!

Any questions?

Audrey’s Group

Observing an Exoplanet

Mentor(s): Audrey Omand
Mentees: Ryan Chang, Sean Johnson, Andrea Juarez Nava, Jeslyn Liu, Madison Melendez, Milo Richard

Table of Contents

Research Question

Can we identify a TESS light curve that:

- Features a transit depth that is detectable by the Leuschner Observatory
- Has a period that is short enough for us to observe it multiple times within our timeline
- Has a strong signal-to- noise confidence interval

Can we definitively confirm its existence within its timeline? Could we potentially determine its atmospheric composition using Leuschner's spectrometer?

Background

Our research project will use the Leuschner Observatory to observe potential exoplanet candidates found by the TESS satellite.

Leuschner Observatory:

- Located in Lafayette, CA and can be remotely operated from UC Berkeley and SFSU
- Has two main telescopes
  - Optical telescope used for infrared astronomy
    - Will be remotely controlled from Campbell Hall for this project
  - Radio telescope for radio astronomy

Optical Telescope Features

- 30-inch (76 cm) aperture
- SBIG STL-11000 CCD camera
- UBVRI photometer
- Spectrograph
- Fabry-Perot spectrometer

Methodology

- Our project will consist of three stages
- Filing through thousands of qlp (quick-look pipeline from MIT)
  - Determine what ***could*** be an exoplanet based on specific characteristics
  - Holistic assessment

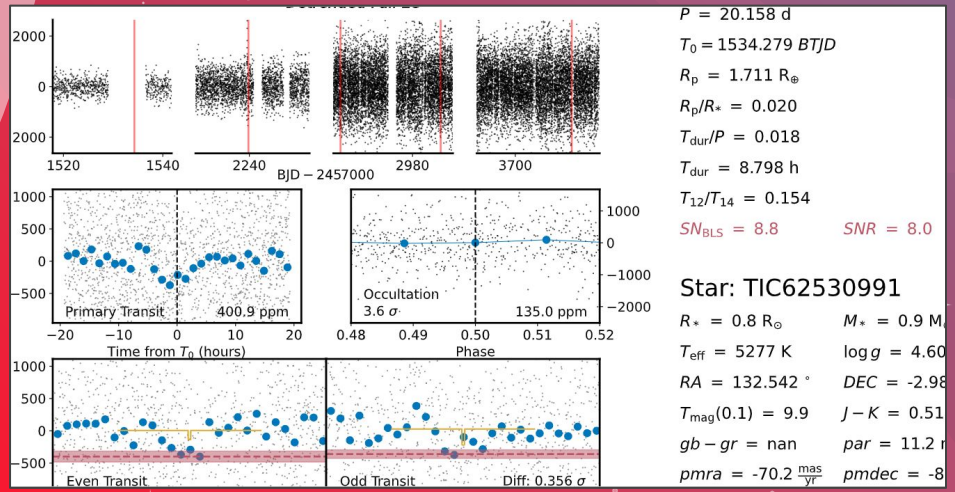

Not an exoplanet

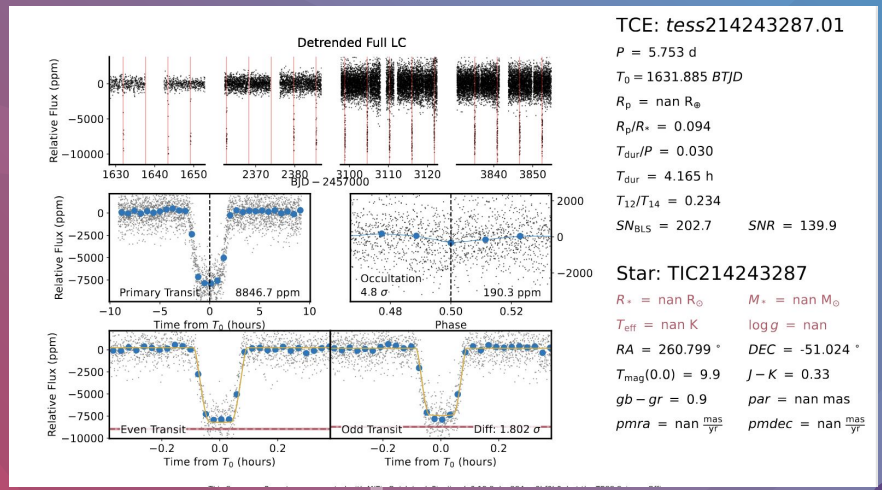

Potentially an exoplanet

Our Top Candidate

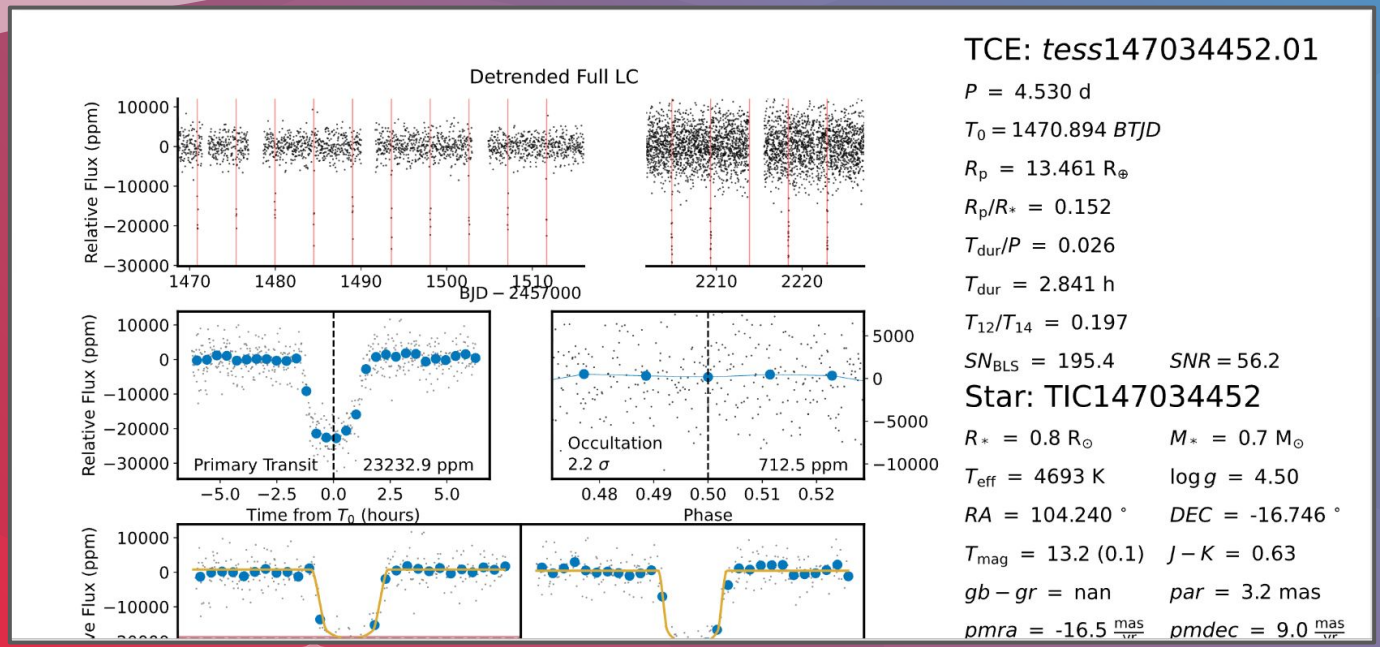

TCE: *tess*147034452.01

P = 4.530 d

T_0 = 1470.894 *BTJD*

R_p = 13.461 $R_\oplus$

R_p/R_* = 0.152

T_{dur}/P = 0.026

T_{dur} = 2.841 h

T_{12}/T_{14} = 0.197

SN_{BLS} = 195.4 SNR = 56.2

Star: TIC147034452

R_* = 0.8 $R_\odot$ M_* = 0.7 $M_\odot$

T_{eff} = 4693 K $\log g$ = 4.50

RA = 104.240 ° DEC = -16.746 °

T_{mag} = 13.2 (0.1) $J-K$ = 0.63

$gb-gr$ = nan par = 3.2 mas

$pmra$ = -16.5 $\frac{mas}{yr}$ $pmdec$ = 9.0 $\frac{mas}{yr}$

Methodology (cont.)

- Next, we will observe the object through multiple periods of transit with the Leuschner observatory and collect data
- Use Python as well as other methods such as dark subtraction and flat division to simplify and clean data
- Report findings

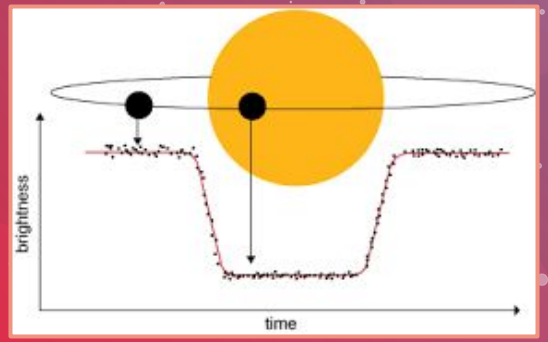

Transit Method

PICTURES ON NEXT TWO SLIDES

The “transit method” allows for the detection of exoplanets via observation of their host stars’ light curves.

An object, such as an exoplanet, passing in front of (or “transiting” across) a star will cause a dip in the star’s light curve. Exoplanets, in particular, lend themselves to U-shaped dips.

Transiting Exoplanet Survey Satellite (TESS)

- NASA-sponsored, MIT-led
- Still active
- Orbits the earth in a highly elliptical and P/2 lunar-resonant orbit (i.e., TESS completes two orbits for one lunar orbit)
- Features four highly-optimized, red-optical-sensitive, wide-field cameras
- As of October 13, 2025, TESS has confirmed ~705 exoplanets

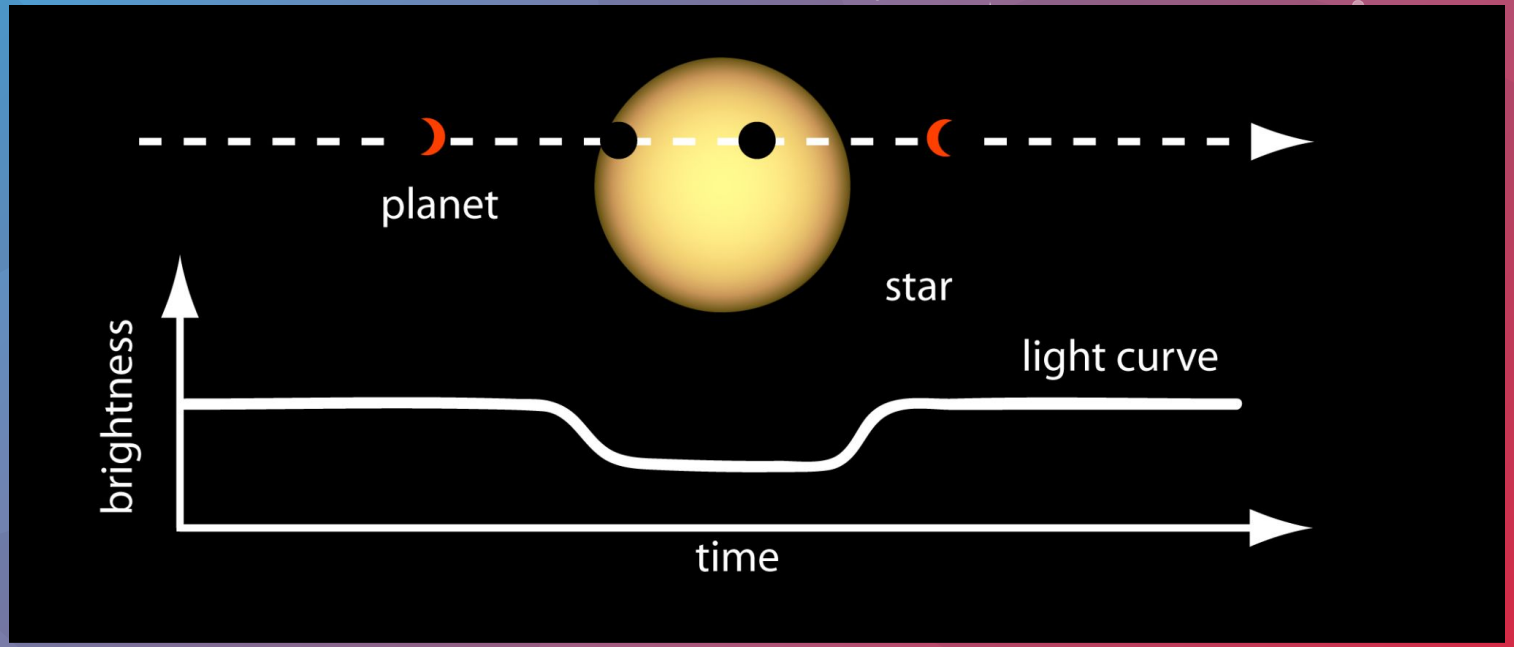
planet
star
light curve
brightness
time

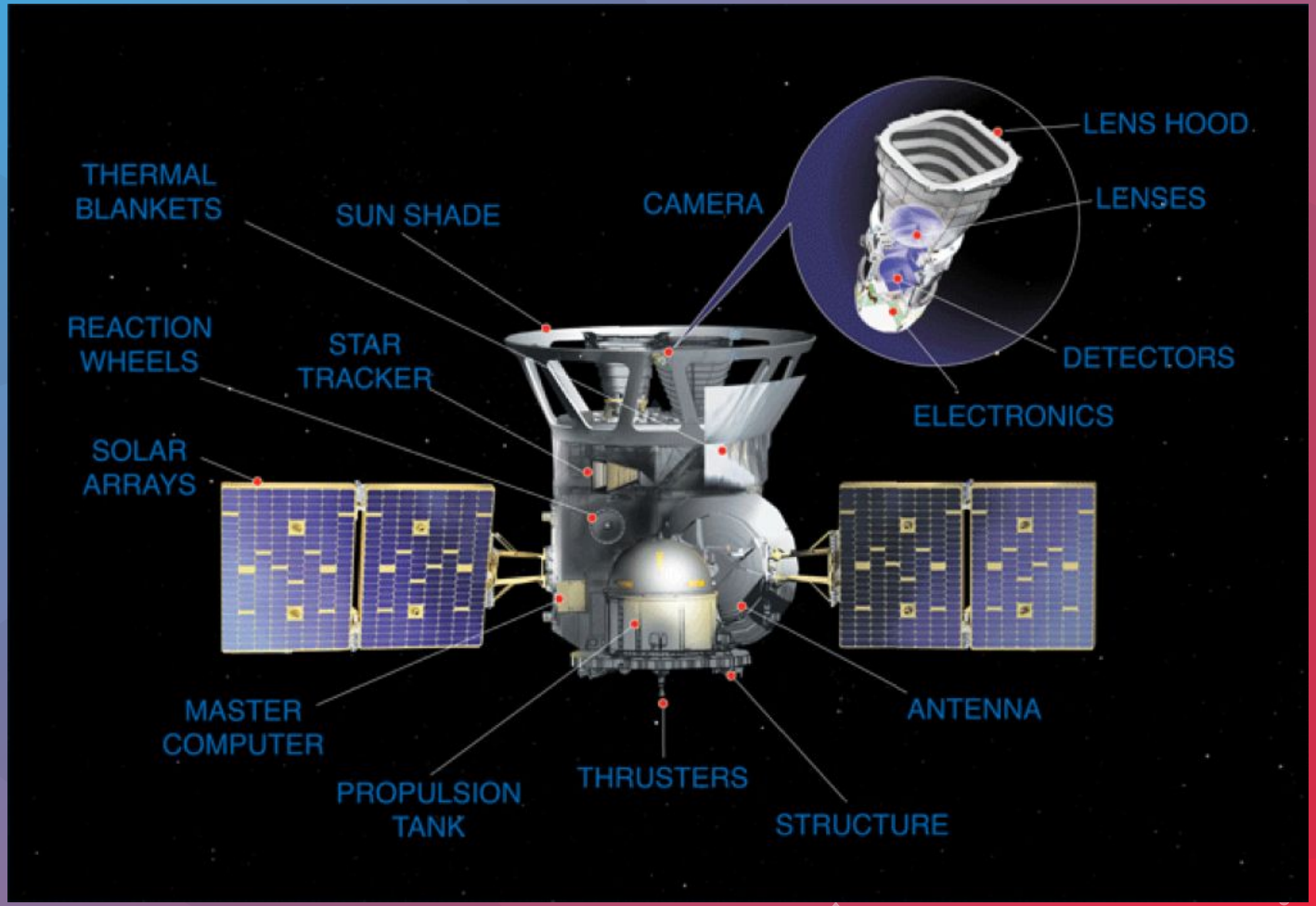
LENS HOOD
LENSES
CAMERA
THERMAL BLANKETS
SUN SHADE
REACTION WHEELS
STAR TRACKER
DETECTORS
ELECTRONICS
SOLAR ARRAYS
MASTER COMPUTER
ANTENNA
PROPULSION TANK
THRUSTERS
STRUCTURE

Progress So Far

- Searched through thousands of TESS signals for potential signatures
- Cross-referenced potential candidates using SIMBAD for flagged false positives, existing exoplanets
- Identified top candidate for observation

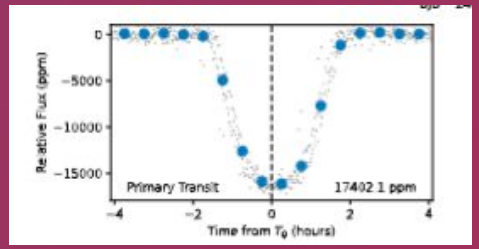

Query : TIC73723286

Basic data :

CD-39 6337 -- Spectroscopic Binary

Other object types:	* (CD,CF,...), **SB*** (2022yCat), **PM*** (2016A&A), **NIR** (2MASS)
ICRS coord. *(ep=J2000) :*	**10 22 32.8568543448 -40 30 58.191129828 (Optical) [0.0077 0.0094 90] A** 2020yCat.1350....0G
FK4 coord. *(ep=B1950 eq=1950) :*	10 20 22.6395776731 -40 15 44.888471661 [0.0077 0.0094 90]
Gal coord. *(ep=J2000) :*	274.6363291027174 +14.0357150659568 [0.0077 0.0094 90]
Proper motions *mas/yr* :	**39.020 -42.455 [0.010 0.012 90] A** 2020yCat.1350....0G
Radial velocity / Redshift / cz :	**V(km/s) -46.43 [2.26] /** z(spectroscopic) -0.000155 [0.000008] **/** cz -46.43 [2.26] **(Opt) C** 2018yCat.1345....0G
Parallaxes *(mas)*:	**7.6303 [0.014] A** 2020yCat.1350....0G
Spectral type:	**G5 E** 2014yCat....1.2023S
Fluxes (6) :	**B 10.54 [0.03] D** 2000A&A...355L..27H **V 9.76 [0.02] D** 2000A&A...355L..27H **G 9.581756 [0.002767] C** 2020yCat.1350....0G **J 8.499 [0.021] C** 2003yCat.2246....0C **H 8.193 [0.057] C** 2003yCat.2246....0C **K 8.093 [0.024] C** 2003yCat.2246....0C

Timeline - Next steps

Winter Break

Choose our exoplanet, find out when transit parameters were optimal, check with the professor availability to start observing

January

Begin observing the transit. Schedule observations at Campbell

March

Analyze the recovered data from the Leuschner telescope and compare it with the TESS data

April

Organize, publish and present our findings to mentors, students and faculty

Feasibility

Available Resources

- **Leuschner telescope**
  - Ground base observatory depends on ideal weather conditions and functionality of the telescope during transit period
- **Time**
  - Choosing a definite candidate and how much we time we take, affect when we are doing our first observation
  - Transit period and orbital period given by TESS → hinders the possibility of having sufficient observations

Budget

FREE!!!

Citations

References

1) Kaushik M. et.al. Exoplanet detection: A detailed analysis. arXiv, pages 1–8, 2024.
2) N. M. et al. Guerrero. The tess objects of interest catalog from the tess prime mission. The Astrophysical Journal Supplement Series, 254(2):39, 2021.
3) C. et al. Huang. Photometry of 10 million stars from the first two years of tess full frame images: Part i. Research Notes of the AAS, 4(11), 2020.
4) C. et al. Huang. Photometry of 10 million stars from the first two years of tess full frame images: Part ii. Research Notes of the AAS, 4(11), 2020.
5) J. et al. Jenkins. The tess science processing operations center. Proceedings of the SPIE, 9913(20), 2000.
6) M. et al. Kunimoto. The tess faint-star search: 1617 tois from the tess primary mission. The Astrophysical Journal Supplement Series, 259(2), 2022.
7) G. et al. Olmschenk. Identifying planetary transit candidates in tess full-frame image light curves via convolutional neural networks. The Astrophysical Journal, 161(6), 2021.
8) J. N. Winn. Transits and Occultations. In Sara Seager, editor, Exoplanets, pages 55–77. University of Arizona Press, 2010.

Caitlin’s Group

Bending Space, Time, and Light: Microlensing Prediction Curves with PyTorch

Emilio Acosta, Hannah Eghtedari, Lily Myers, Joseph Ong, Andrew Wang, Sky Xu

Mentor: Caitlin Begbie

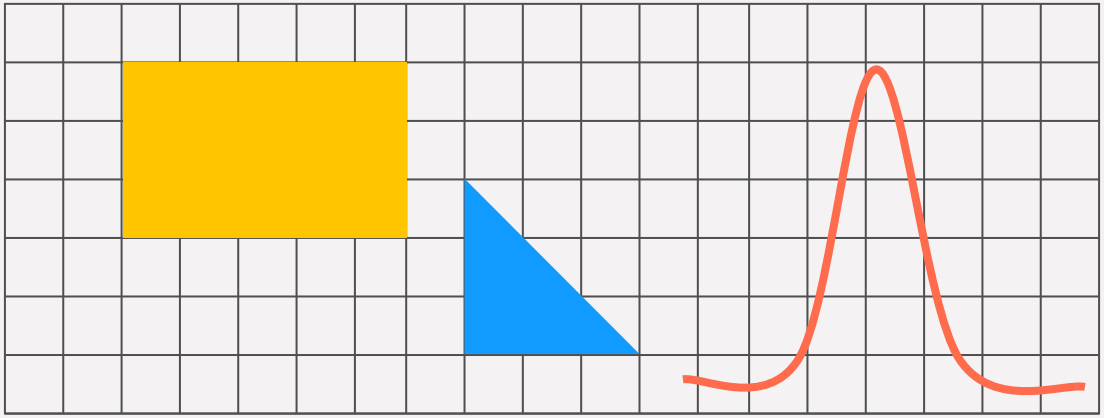

Background

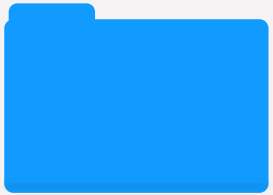

Research Question

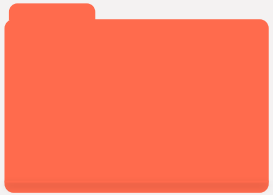

Methods

Timeline

Background

- Microlensing[1] occurs when light from a source bends around a massive object that passes between the source and observer
- The object's gravity acts as a lens, magnifying the light from the source
- During microlensing events, we can detect and measure the flux, or brightness of the source over time
- Analyzing microlensing curves allows us to infer properties of the lens such as its mass or distance from Earth
- Microlensing can help identify bodies that emit little light, such as planets, brown dwarfs, and black holes

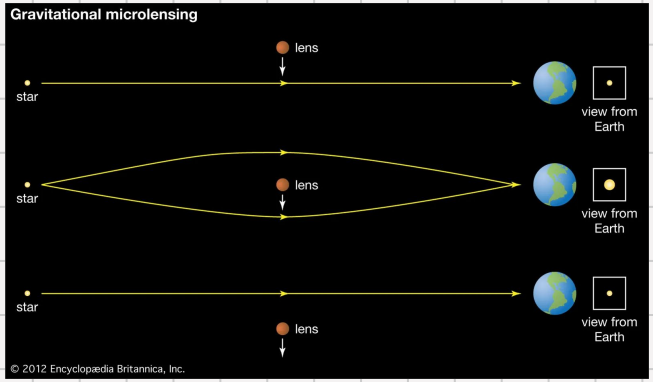

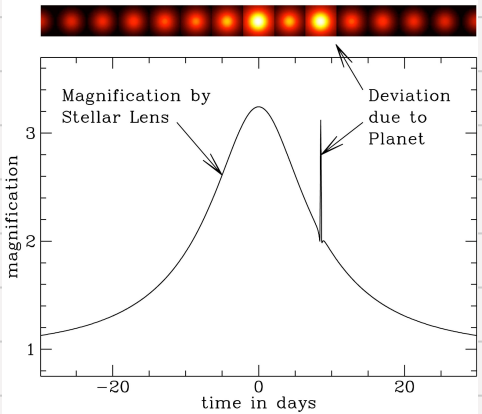

Background

- Machine learning is defined as training a computer to complete a task but not explicitly coding it in, rather the computer learns off inputs and is rewarded when outputting the correct answer.
- We will be using PyTorch[2], a package in Python which can perform machine learning. It has built-in neural networks to adapt to data and minimize loss[3].
- Other modules exist like TensorFlow which is more expansive, but PyTorch fits better for the time frame of this project.
- We will be using an RNN (Recurrent Neural Network), namely, an LSTM (Long Short Term Memory) for our data.
- RNNs are based off sequence-based data, which is where data from the past is used to predict the future. LSTMs use both recent and long-term memory to predict the future.
- Flux-time graphs, the ones we get from microlensing events, are perfect examples of sequence-based models, so RNNs and LSTMs work perfectly.

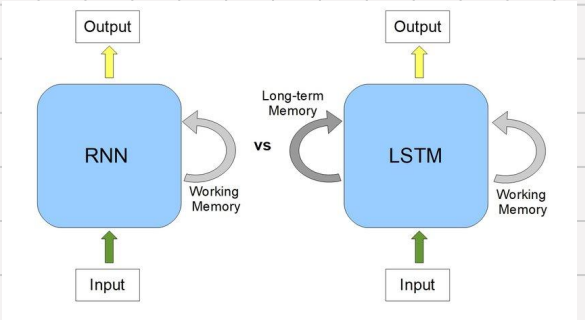

PyTorch

Research Question

★ What aspects of a microlensing light curve are most important for understanding and predicting single-lens events?

The key features are the baseline brightness, the rise toward the peak, and the peak itself. These show how the lensing effect strengthens as the source and lens move into alignment. By looking at how fast the brightness increases and how the peak forms, we capture the basic pattern the model needs to learn to predict the rest of the event[4].

Research Question

★ How can we use machine learning to predict microlensing curves in single-source, single-lens events?

We can train a model using PyTorch based on past microlensing light curves so it can learn how these events typically evolve, and then we use that trained model to predict how an ongoing event will continue in the near future.

Methods

Collecting Data

- Using open-source data sets from OGLE[5] (Optical Gravitational Lensing Experiment) and potentially GAIA
- Creating two sets of data, one for training the model and another for testing it
  - Training data will be full light curves while testing data will be “incomplete” light curves
  - Might create even more data sets for refining model

Testing and Training

- Assign training data to the majority of the completed events
- Assign testing data to the remaining completed events and cut off a portion of the curve to test our model’s prediction
- Compare the testing results to the real results and refine our model from there
- Finally, we hope to apply this model on ongoing events

Timeline

Start Date	Goals
Break Dec 22	Winter Break: Take 25-Hour PyTorch Course[6]
Wednesday Jan 21	Review and OGLE Data Collection
Monday Feb 2	Build Testing/Training Datasets
Monday Feb 16	Build PyTorch LSTM model with Training Data

Start Date	Goals
Monday Mar 2	Test Model with Synthetic Data
Monday Mar 16	Refine Model For Accuracy (As Needed)
Monday April 6	Apply Model: Predictions and Margin of Error
Monday May 4	Final ULAB Project Presentations

References

[1]Shude Mao. Introduction to gravitational microlensing, 2008.

[2]Adam Paszke, Sam Gross, Francisco Massa, Adam Lerer, James Bradbury, Gregory Chanan, Trevor Killeen, Zeming Lin, Natalia Gimelshein, Luca Antiga, et al. Pytorch: An imperative style, high-performance deep learning library. Advances in neural information processing systems, 32, 2019.

[3]Brad Heintz. Introduction to pytorch – youtube series. https://docs.pytorch.org/tutorials/beginner/introyt/introytindex.html, 2025. Accessed: 2025 – 12 – 03.

[4]Street, Rachel, et al. *Introduction to Microlensing — What Is Microlensing?* Microlensing Source, 2025, https://www.microlensing-source.org/concept/.

[5]Andrzej Udalski, Micha l Krzysztof Szyma´nski, and Grzegorz Szyma´nski. Ogle-iv: fourth phase of the optical gravitational lensing experiment. arXiv preprint arXiv:1504.05966, 2015.

[6]freeCodeCamp, *PyTorch Course*

Chuyun’s Group

Halim’s Group

Distant Kuiper Belt Object (KBO) Clustering and its Relationship to the Ninth Planet Hypothesis

Iris Shi, Hillary Tian, Bryan Ramirez,
Alexander Huang

Outline:

1. Brief Introduction
2. Background
3. Research Question
4. Methodology
5. Resources and Libraries
6. Timeline

What’s beyond Neptune in our Solar System?

- Wobbles in Uranus led to **Neptune** being discovered in 1781 by Scientist Herschel
    - Scientist Le Verrier’s mathematical predictions let to immediate discovery through observation
- **Pluto** - but reclassified as a dwarf planet
- **Kuiper Belt objects** - beyond the gas giants

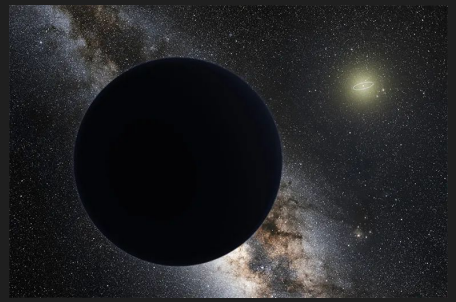

FOR CENTURIES, HUMANS HAVE ALWAYS BEEN CURIOUS WHAT ELSE IS IN THE OUTER SOLAR SYSTEM?

Natural question: Could there be another planet beyond our 8 planet system?

Allow us to introduce the current unexplained phenomena ->

Background: The Solar System

-Trans Neptunian Objects TNOs are the broad category of objects gravitationally bound to the sun whose semimajor axes lie beyond 30 AU

-Classical Kuiper Belt 30-50 AU.

-Scattered Disk overlapping, sparse, more eccentric, and further out

-Sedna-like planets (highly inclined, eccentric and semi-major axis >50AU

(Wikipedia n.d.)

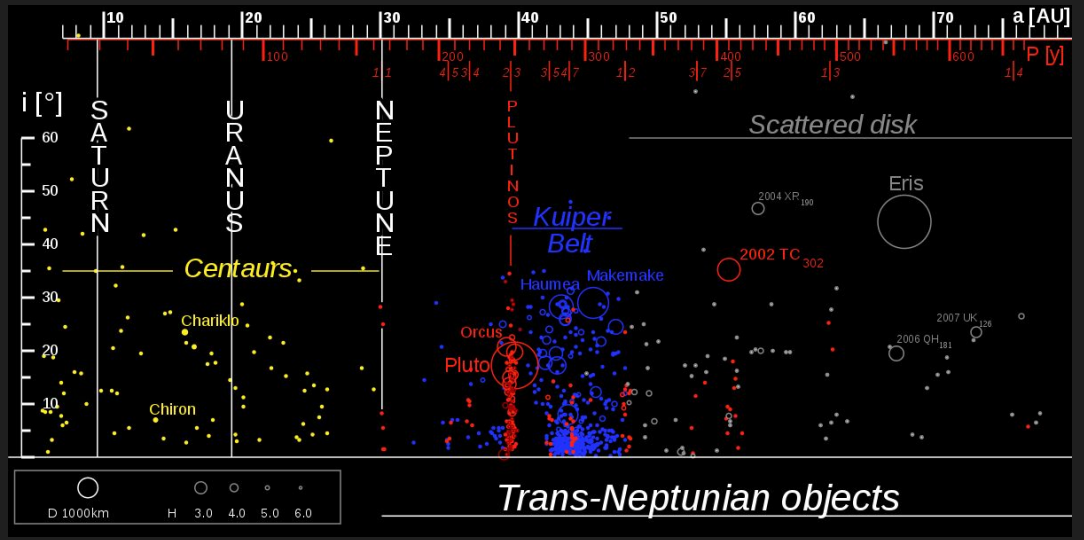

(Catalina Sky Survey n.d.)

Helpful diagrams

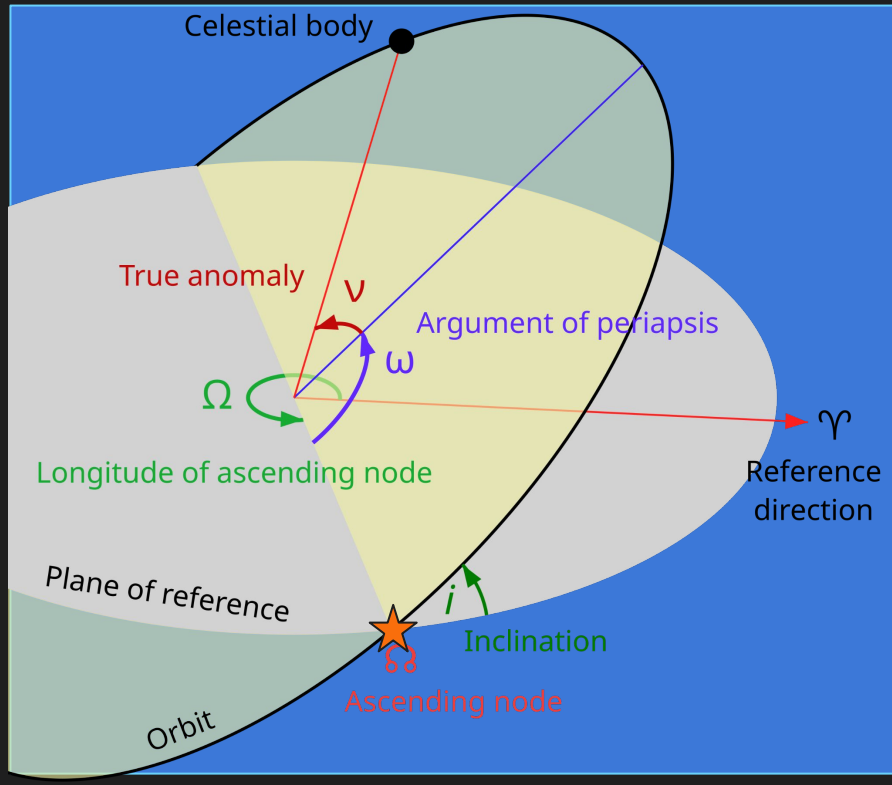

Inclination

Argument of Periapsis - General term for argument of perihelion (rotation in its own plane)

Longitude of the Ascending Node - orientation of the ascending node with respect to the vernal equinox

Longitude of Perihelion - The sum of the previous two orbital elements

Background: Anomalous Clustering

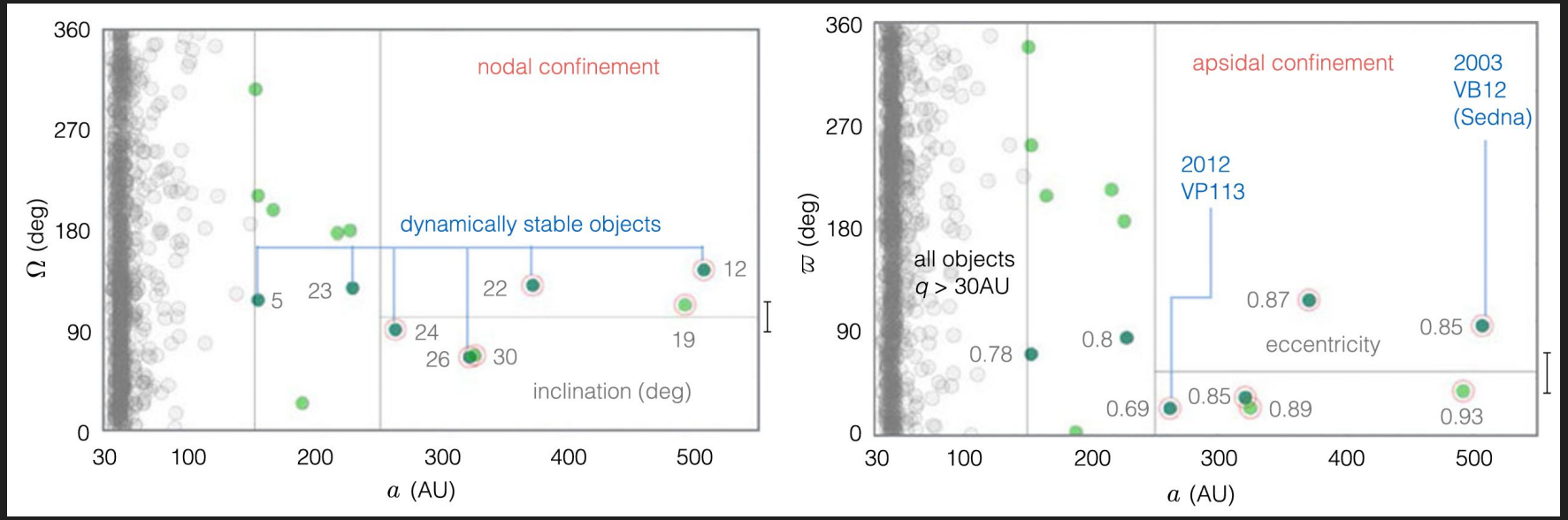

(Batygin 2016)

-Nodal confinement = orbital pole alignment
-Apsidal confinement + Nodal confinement = perihelion direction alignment
-Does not align with age of solar system and differential precession
-0.007% chance of observed clustering based on TNOs
-Observational bias does not explain clustering (longitudinal indifference, 6 surveys)

Research Question

Are the anomalous orbits of Kuiper Belt Objects best explained by the Ninth Planet hypothesis, or does new data suggest alternative explanations for the unexpected clustering?

- The Ninth Planet Hypothesis is our **guiding framework**
- Direct observation is currently infeasible, but new telescope datasets are promising
- WHAT WILL BE NEW - ***10 yrs of new datasets***, *parameters, new techniques (machine learning...) and cross-comparison to other "opposing" hypotheses.*

Why did we choose this route?

a) Continue work of Batygin & Brown, making Ninth Planet Hypothesis more conclusive
   i) Improve odds of detection and the likelihood of the existence of the Ninth Planet, constraining parameters
   ii) Understand our data better (useful for any hypothesis or astrophysical theory development)
      1) Useful for any hypothesis (e.g. Solar System formation theories)

Method: *3 branches, 1 tree*

1. Data

Databases

- Vera Rubin Observatory @ Chile: NEW 2026 release (10 yrs)
- Subaru telescope -20 yr up to 2023
- GAIA - 2016 + 2022
- observation from Hawaii
- NASA - Citizen project 2017
- Eliminate parameters
- Likelihood function of parameters

Data analysis

- K-Means unsupervised clustering algorithm for exploratory data analysis
  - Machine learning
  - Convoluted Neural Networks
- Comparison with 2016 Batygin EDA

2. Analytical

Theory

- Secular perturbation theory (Gauss averaging)
- Mean-motion resonance
- Hamiltonian
- New parameters
  - Inclination (i)
  - Longitude of ascending node (Ω)

(See slide 5 diagram)

3. Numerical

Direct N-body simulations
Monte Carlo Markov Chain sampling

- Orbital stability
- Avoid grid sampling for 4D parameter space
- Solar System age as limiting case
- Vary from 10 to 15 Earth masses

Generating data in

- Phase portraits
- Fit with real data
- Evolution of orbit and formation (EXTENSION)

Data and simulation **trends** inform direction of mathematical framework

Simulation results informs **effectiveness**, **quality** and **source** of data/analysis

The initial equations in analytical help “guess” the function to fit the data

Methods (Analytical) Secular Perturbation Theory

Gauss's Averaging Method

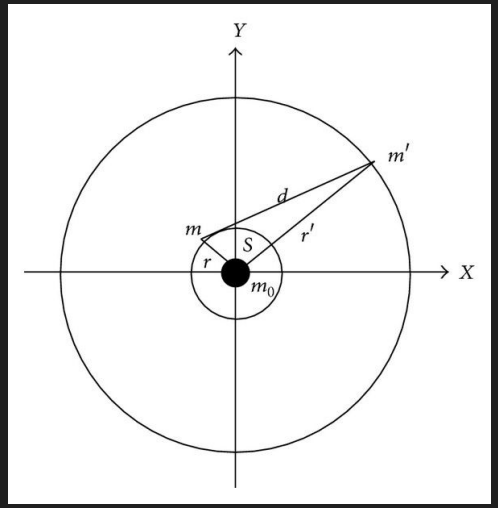

(Wiley Library n.d.)

Long Term Effects

Differential precession and stability

(Batygin 2016)

$$\mathcal{H} = -\frac{1}{4}\frac{\mathcal{G}M}{a}(1-e^2)^{-3/2}\sum_{i=1}^{4}\frac{m_i a_i^2}{Ma^2} - \frac{\mathcal{G}\,m'}{a'}\left[\frac{1}{4}\left(\frac{a}{a'}\right)^2\frac{1+3\,e^2/2}{(1-(e')^2)^{3/2}} - \frac{15}{16}\left(\frac{a}{a'}\right)^3 e\,e'\frac{1+3\,e^2/4}{(1-(e')^2)^{5/2}}\cos(\varpi'-\varpi)\right],$$

Methods (Data + Numerical)
K-means unsupervised + Markov Chain Sampling

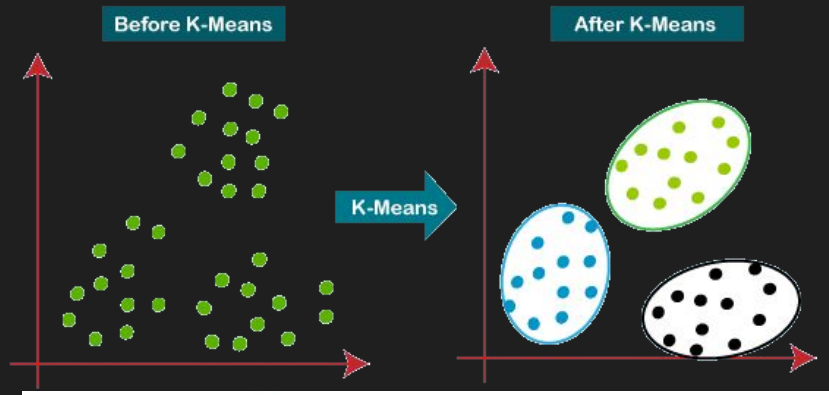

number of clusters
number of cases
centroid for cluster j
case i

$$\text{objective function} \leftarrow J = \sum_{j=1}^{k} \sum_{i=1}^{n} \left\| x_i^{(j)} - c_j \right\|^2$$

Distance function

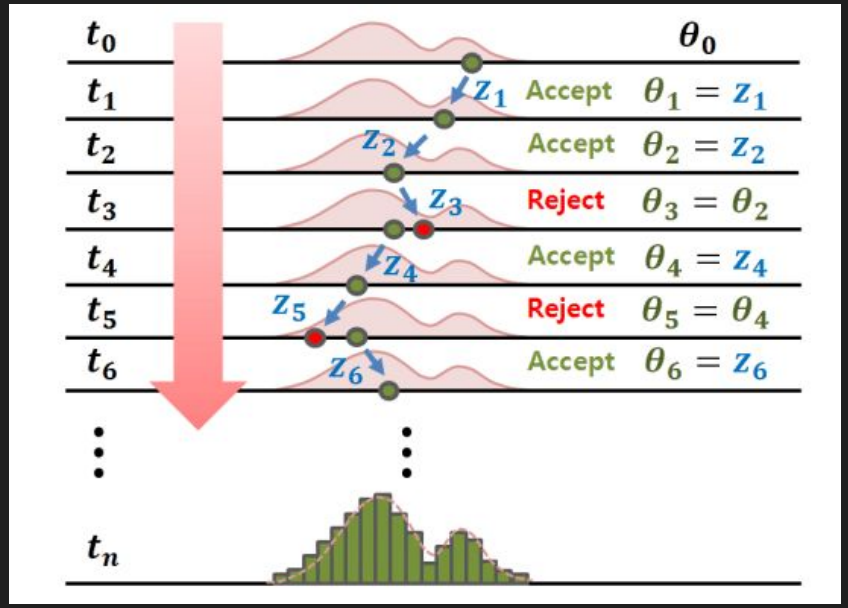

-We will use K-means clustering to quantify the distribution of KBOs in parameter space.
-Try to identify dynamical reason for observed clustering.
-Construct prior function from K-means and analytical theory.

Budget, resources, collaborations

(Possible) budget: $100 minimum for life+mental support (quote: “Boba” - Halim Perez :])

Resources (build simulation w/):

- Python
- Packages:
  - Astroquery (JPL.HORIZONS, Minor Planet Center, etc.)
  - Rebound (simulation)
  - SciPy
  - MatPlotLib
  - Pandas
  - Astropy
- N3AS Supercomputing - Mentor Halim

Collaborations:

- NONE SO FAR!!!
- Potentially contacting Batygin & Brown at Caltech to present findings

Demo N-body Simulations (Visuals with MatPlotLib)

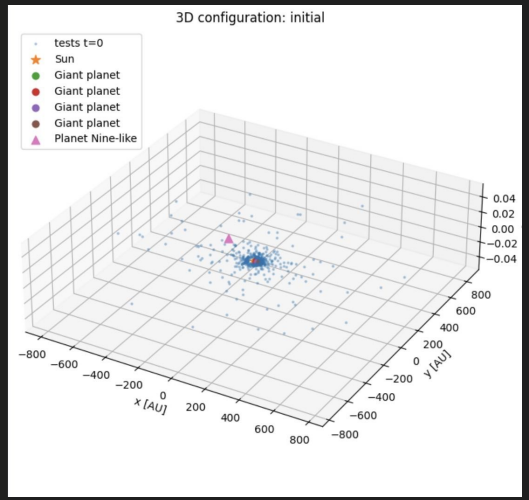

Initial Setup

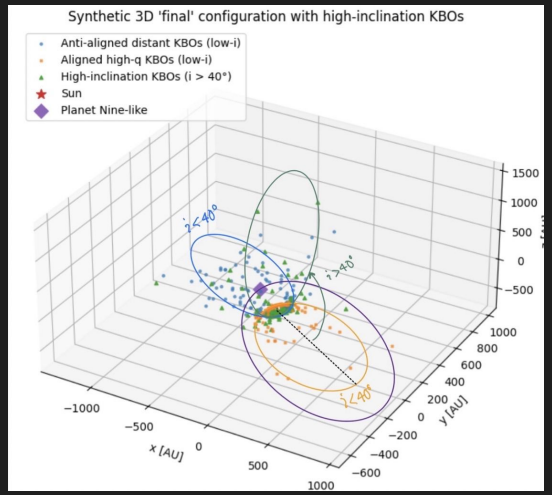

First Result

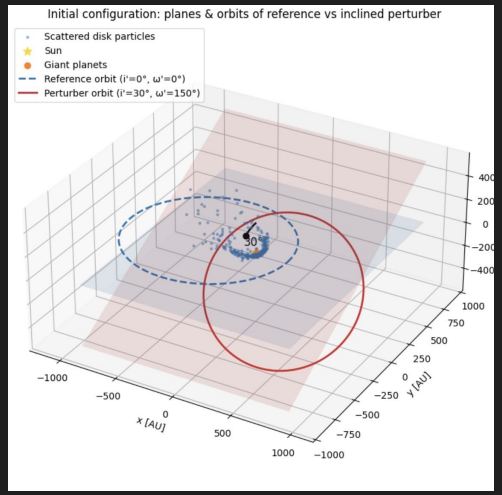

Inclination Variations

Timeline

Winter Break →

We will continue independent research study (we WILL be enjoying our winter break)

1/12–1/25 →

Query astronomical databases for KBO data & derive equations for understanding to determine analytical framework

1/26–2/08 →

Begin EDA and use software to replicate simulations from *Batygin & Brown (2016)* for consistency and identify patterns to use in our methods

2/09–2/22 →

Construct the N-Body simulation with rebound, keeping our understanding in mind to reduce bias,

2/23–3/07 →

Run Simulation under different scenarios and control scenarios for alternative explanations, and make statistical comparisons between simulated and real clustering scenarios.

3/08–3/21 →

Use MCMC to sample from the parameter space and create likelihood function for stability.

AND Start paper writing

3/22–4/04 →

We will integrate simulation outputs with analytical predictions and observational datasets to produce a cohesive scientific narrative; finalize the scientific argument and synthesize the implications for the Planet Nine hypothesis

4/05–4/18

Compile all data and figures into research paper

References

Batygin, K. (2017). Dynamical Evolution Induced by Planet Nine. The Astronomical Journal.

Bottke, W. F. (2023). The Collisional Evolution of the Primordial Kuiper Belt, Its Destabilized Population, and the Trojan Asteroids. The Planetary Science Journal.

Brown, K. (2023). Modified Newtonian Dynamics as an Alternative to the Planet Nine Hypothesis. The Astronomical Journal, 166(4).

Chadwick, T. A. (2014). A Sedna-like body with a perihelion of 80 astronomical units. Nature.

Levison, H. (2008). Origin of the Structure of the Kuiper Belt during a Dynamical Instability in the Orbits of Uranus and Neptune. Icarus, 196(1).

Li, J. (2020). Mean plane of the Kuiper belt beyond 50 AU in the presence of Planet 9. Astronomy and Astrophysics, 637.

Scattered disc - Wikipedia. (n.d.). Wikipedia, the free encyclopedia. Retrieved December 7, 2025, from https://en.wikipedia.org/wiki/Scattered_disc

What is a Trans Neptunian Object? | Catalina Sky Survey. (n.d.). Catalina Sky Survey. Retrieved December 7, 2025, from https://catalina.lpl.arizona.edu/faq/what-trans-neptunian-object

Planet Nine. (n.d.). In Wikipedia. Retrieved December 7, 2025, from https://en.wikipedia.org/wiki/Planet_Nine

Astrum. (2023, November 7). Are we close to finding Planet 9? [Video]. YouTube. https://www.youtube.com/watch?v=FYbhzDJT6Ms

Lista, L. (2023). Statistical methods for data analysis: With applications in particle physics (3rd ed.). Springer. https://doi.org/10.1007/978-3-031-19934-9

Thank you!

Questions?

Mariam’s Group

Sulfur-bearing Molecules in MAPS Protoplanetary Disks

Mentor: Mariam Helal

Mentees: Kaidren Alexander Clark, Francesca Chan Estrada, Aryan Jain, Annecy Jiang, Weikang Lao, Arshia Tomar

Table of contents

01

Background

Background

- Gas and dust-rich structures surrounding young stars where planets form
- Chemistry comes from both the parent molecular cloud and internal disk processes
- Forms when a cloud collapses due to gravity overcoming internal pressure
    - **Jean's mass/Jean's length**
- **Inner Disk**: hot, dense, strong radiation, chemically active
- **Outer Disk**: cold, low density, molecules freeze
- **Upper Layers**: high radiation, gas-phase molecules
- **Midplane**: cold, dense, ices and solids common

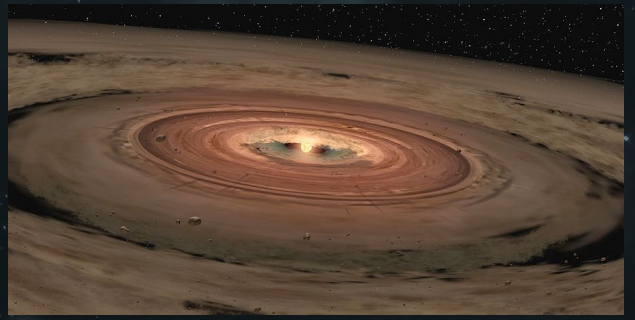

NASA/JPL-Caltech/T. Pyle (SSC)

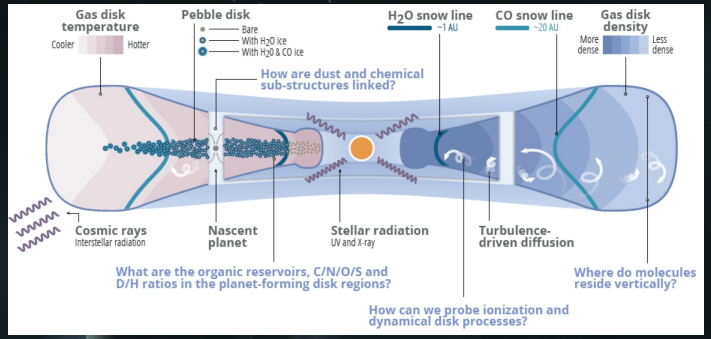

Öberg & Bergin 2021

Why Study Sulfur?

- Understanding where sulfur resides helps reveal the process of how chemicals are delivered to forming planets
- Investigate how sulfur becomes a part of the atmosphere and organics (potential life on exoplanets)
- Analytically, can assist with determining:
  - The local gas-phase C/O ratio, which strongly determines whether sulfur forms CS or SO
  - UV and X-ray radiation, which is the key driver for photodissociation
  - Temperature, which controls freeze-out of sulfur molecules

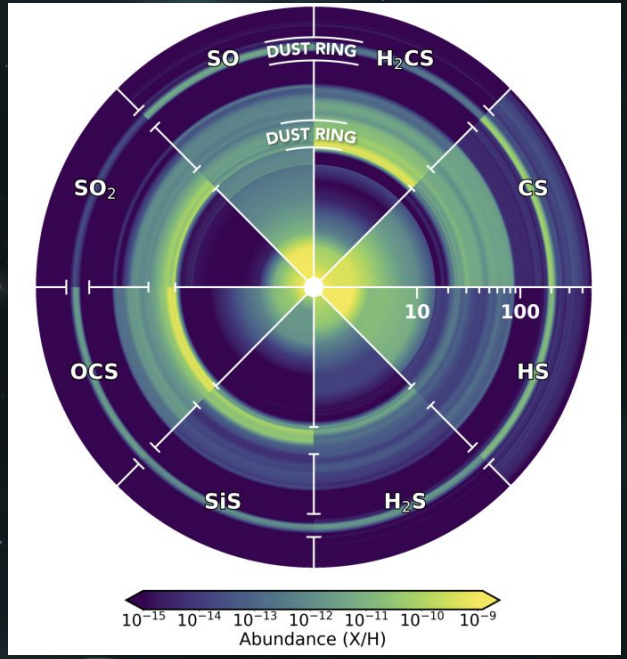

Keyte et al. 2023

02

Research Question

Motivation

- Our overall goal is to examine sulfur-bearing molecules across various MAPS disks and evaluate how their abundances vary with stellar and disk properties
- Molecules of interest: CS, SO, C_2S, & H_2S
  - CS → typical most abundant sulfur-bearing molecule in the gas phase
  - C_2S → particularly sensitive to environmental processing and chemical inheritance
- Comparing sulfur across disks provides insight into disk structure, chemical inheritance, and the partitions of volatile & refractory sulfur

Table 1
Stellar and Disk Properties as Presented in Öberg et al. (2021)

Source	Spectral Type	Dist. (pc)	Incl (deg)	PA (deg)	$T_{\rm eff}$ (K)	L_* ($L_\odot$)	Age[a] (Myr)	M_*[b] ($M_\odot$)	$\log_{10}(\dot{M})$ ($M_\odot$ yr^{-1})	$v_{\rm sys}$ (km s^{-1})	References
IM Lup	K5	158	47.5	144.5	4266	2.57	∼1	1.1	−7.9	4.5	1,2,3,4,5,6
GM Aur	K6	159	53.2	57.2	4350	1.2	∼3–10	1.1	−8.1	5.6	1,7,8,9,10,11,12
AS 209	K5	121	35.0	85.8	4266	1.41	∼1–2	1.2	−7.3	4.6	1,2,6,13,14
HD 162396	A1	101	46.7	133.3	9332	17.0	≳6	2.0	−7.4	5.8	1,2,6,15,16
MWC 480	A5	162	37.0	148.0	8250	21.9	∼7	2.1	−6.9	5.1	1,17,18,19,20,21

Öberg et al. 2021

By tracking sulfur-bearing molecules across protoplanetary disks with different physical properties, what trends can we observe, and what do these trends reveal about the disks' physical and chemical conditions?

Key Assumptions

1. Gas-phase sulfur representation:
    a. Detected sulfur-bearing molecules represent most observable gas phase
    b. DM Tau → only few sulfur species are detectable
    c. Even without full wavelength coverage, the species we observe capture a meaningful fraction of the relative sulfur abundance
2. Nondetections:
    a. Many sulfur transitions are intrinsically faint
    b. These provide upper limits on abundance
        i. Upper limits indicate whether sulfur is: scarce, locked in solids/ices, or not efficiently produced
3. LTE, Excitation, & Optical Depth:
    a. Assume LTE → molecular level populations follow a Boltzmann distribution
    b. Adopt single excitation temperature → convert line intensities to column densities
    c. Assume optical thinness → observed intensity is directly proportional to true molecular abundance

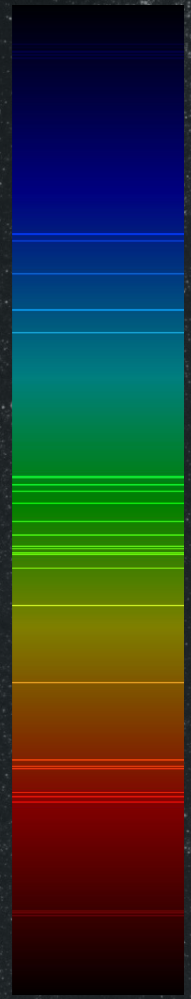

McZusatz, Wikimedia Common

Expected Outcomes & Hypothesis

- We expect systematic differences in gas-phase abundances across different MAPS disks
- These differences likely reflect variations in sulfur chemistry, environmental processing, and initial chemical conditions
- Some disks may retain more sulfur in the gas phase, while others may be locked into solids or iceas more efficiently

03

Methods

Methods

- Data: ALMA MAPS survey of five disks
- Target molecules: CS, SO, C_2S, & H_2S
- Spectral Extraction: Data cubes analyzed in CARTA, spectra extracted at sulfur transition frequencies
- Line Identification and modeling: CASSIS used to confirm lines and fit LTE models
- Column Densities and trends: Calculated in Python and compared across disks to test sulfur abundance trends

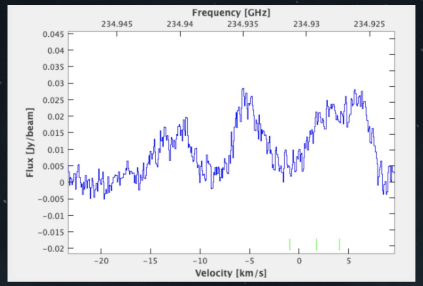

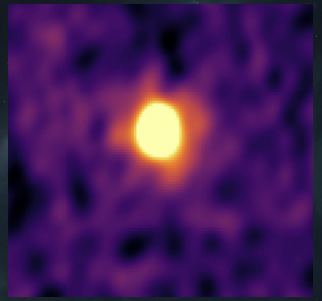

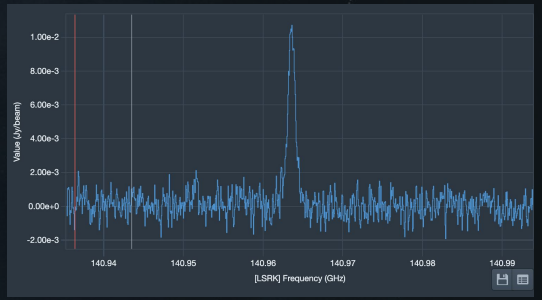

04

Budget & Resources

Budget and Resources

- Unlikely to need any expenses for our project
- Possibility of needing more storage space to hold large data sets
  - May utilize the computers at the PIL
- We use public databases such as Splatalogue to identify the molecular transitions and the ALMA archive to download the data of protoplanetary disks
- CARTA and CASSIS are used for analysis

05

Timeline

Timeline

1/20–1/30: Use Splatalogue to compile information (key transitions) to figure out what datacubes to download based on frequency from the ALMA archive and distribute disks

2/4–2/27: Each person uses CARTA for spatial analysis to search and extract any spectral peaks, then finding the molecules creating the peaks using CASSIS, making sure to correct for source velocities of individual disks

3/2–3/27: Calculate integrated-flux column densities based on extracted spectra in Python, and verify via LTE modeling in CASSIS. Analyze the resulting abundances to create final visualization plots (ex. moment 0 maps, continuum maps, etc)

3/30–4/10: Make a conclusion about the effects of sulfur-bearing molecules throughout the stages of our protoplanetary disks.

4/13–4/24: Create final deliverables

06

References

References

Kama, Mihkel et al. (Nov. 10, 2019). “Abundant refractory sulfur in protoplanetary disks”. In: The Astrophysical Journal 885.2, p. 114. issn: 0004-637X, 1538-4357. doi: 10.3847/ 1538-4357/ab45f8.

Keyte, Luke et al. (Dec. 21, 2023). Spatially resolving the volatile sulfur abundance in the HD 100546 protoplanetary disk. doi: 10.48550/arXiv.2312.13997.

Le Gal, Romane, Karin I. Oberg, Ryan A. Loomis, et al. (May 2019). “Sulfur Chemistry ¨ in Protoplanetary Disks: CS and H2CS”. In: The Astrophysical Journal 876.1. Publisher: The American Astronomical Society, p. 72. issn: 0004-637X. doi: 10.3847/1538-4357/ ab1416.

Le Gal, Romane, Karin I. Oberg, Richard Teague, et al. (Nov. 1, 2021). “Molecules with ¨ ALMA at Planet-forming Scales (MAPS). XII. Inferring the C/O and S/H Ratios in Protoplanetary Disks with Sulfur Molecules”. In: The Astrophysical Journal Supplement Series 257. Publisher: IOP ADS Bibcode: 2021ApJS..257...12L, p. 12. issn: 0067-0049. doi: 10.3847/1538-4365/ac2583.

McKee, Christopher F. and Eve C. Ostriker (Sept. 1, 2007). “Theory of Star Formation”. In: Annual Review of Astronomy and Astrophysics 45.1, pp. 565–687. issn: 0066-4146, 1545-4282. doi: 10.1146/annurev.astro.45.051806.110602.

Oberg, Karin I., Stefano Facchini, and Dana E. Anderson (Aug. 18, 2023). “Protoplanetary ¨ Disk Chemistry”. In: Annual Review of Astronomy and Astrophysics 61.1, pp. 287–328. issn: 0066-4146, 1545-4282. doi: 10.1146/annurev-astro-022823-040820.

Oberg, Karin I., Viviana V. Guzm´an, et al. (Nov. 2021). “Molecules with ALMA at Planet- ¨ forming Scales (MAPS). I. Program Overview and Highlights”. In: The Astrophysical Journal Supplement Series 257.1. Publisher: The American Astronomical Society, p. 1. issn: 0067-0049. doi: 10.3847/1538-4365/ac1432.

Semenov, D. et al. (Sept. 2018). “Chemistry in disks. XI. Sulfur-bearing species as tracers of protoplanetary disk physics and chemistry: the DM Tau case”. In: Astronomy & Astrophysics 617, A28. issn: 0004-6361, 1432-0746. doi: 10.1051/0004-6361/201832980.

Williams, Becky J. et al. (Oct. 2, 2025). Investigating the Sulfur Mystery in Protoplanetary Disks Through Chemical Modeling. doi: 10.48550/arXiv.2510.02176.

Thank you!

Tanvi’s Group

Listening to the Sun

Daily HFR Spectrograms

Mentor: Tanvi Batra

Mentees: Harpreet Kaur, Evan Melgar, Audrey Meyer, Nadim Mourad, Dani Valadez

Table of Contents

1 Background

Overview of the Parker Solar Probe Mission & FIELDS Instrument

Parker Solar Probe (PSP):

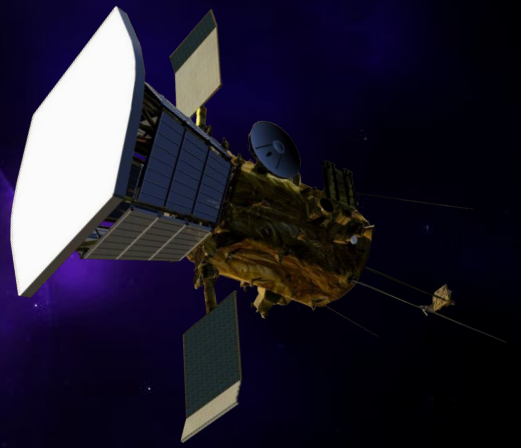

- NASA launched a mission in **2018** to study the Sun up close
- Closest spacecraft in history—within **~10 solar radii**
- Goal: investigate the **solar corona**, **solar wind**, and **magnetic fields** that affect Earth
- Carries multiple instruments, including **FIELDS**, which measures electric & magnetic fields in the solar environment

Why PSP Matters:

- First mission to physically enter the Sun's atmosphere
- Helps explain how the Sun accelerates the solar wind & structures the heliosphere

FIELDS & High-Frequency Receiver (HFR):

Detects radio waves **10 kHz – 19 MHz**

Converts electric-field fluctuations into **Power Spectral Density (PSD)**

PSD shows bursts of radio energy from:

- **Electron beams**
- **Plasma waves**
- **Turbulence** in the inner heliosphere

What this reveals:

- Insights into kinetic processes and **nonthermal particle populations** (Mostafavi et al., 2023)
- Observations of plasma transitions below the **Alfvén critical surface**
- New perspective on how radio emissions evolve as near-Sun conditions change
- Daily HFR spectrograms → track **solar radio activity** and how plasma environments generate/modulate radio emissions

2 Research Question

What are we doing with the PSP and why?

Motivation/Deeper Background

- **Parker Solar Probe (PSP)** provides high-resolution, close-in measurements of these rapid variations.
- **Mostafavi et al. (2024):** PSP/HFR observations reveal detailed transient burst structure and emphasize the need to separate true solar features from instrumental artifacts.
- **Kasper et al. (2021):** PSP's changing heliocentric position and plasma environment significantly affect the brightness of detected emissions.
- **Additional studies (e.g., Guo 2023)** show that propagation effects, spacecraft geometry, and plasma density also shape observed radio power.

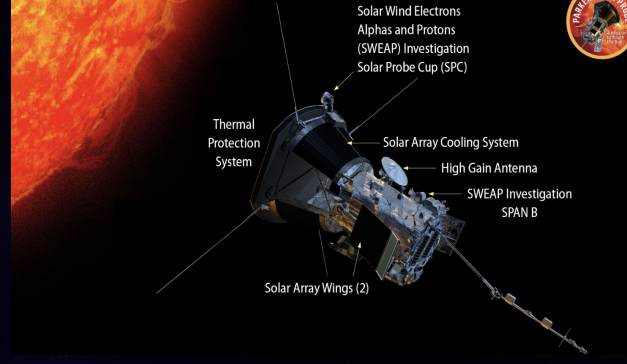

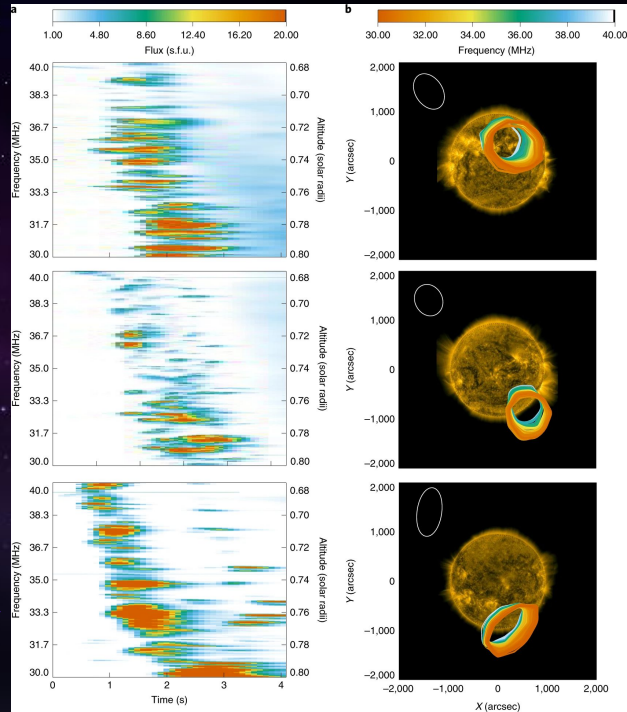

Dynamic spectra of Type III solar radio bursts showing bright, fast-drifting streaks and fine structure.

Research Question

- How does solar radio power vary with time and frequency over the course of a day as measured by the PSP FIELDS High Frequency Receiver, and what physical or instrumental processes produce these variations?

Research Goal/Hypothesis

Goal:

- Identify and interpret patterns in PSP HFR spectrograms that arise from real solar radio bursts, propagation effects, or spacecraft–environment interactions.

Hypothesis:

- The most prominent brightness changes will correspond to transient solar radio bursts.
- Quieter frequency bands will show slower trends influenced by PSP's plasma environment.
- A key part of the analysis is determining how effectively these features can be distinguished from instrumental noise or systematic effects noted in Kasper et al. (2021) and Mostafavi et al. (2024).

3 Methods

FIELDs instrument suite

Consists of
- V1-V4 electric antennas
- V5 voltage sensor
- 1 search-coil magnetometer
- 2 fluxgate magnetometers

Radio Frequency Spectrometer (RFS):
- Solar radio emissions up to 20 MHz are measured on components of the fluctuating electric field (Bale 2016)

We want the high-frequency range (HFR):
~1.6 MHz–19.2 MHz

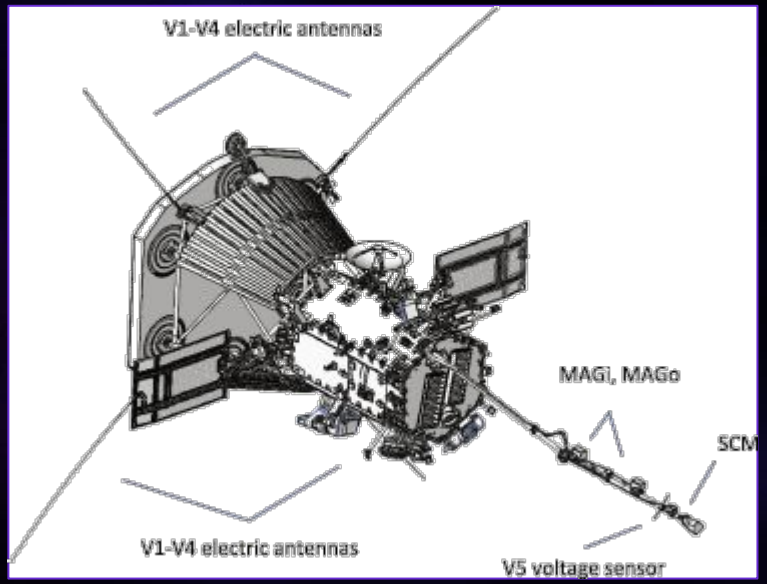

(Bale 2016)

Approach

- If radio brightness depends on both solar activity and PSP's viewing conditions, we expect structured patterns in daily PSP HFR spectrograms.
- Active, burst-rich frequency bands should differ from quiet background bands.
- Instrumental effects (noise, aliasing, gain changes) can mimic real variability; hence, understanding time–frequency evolution is essential.

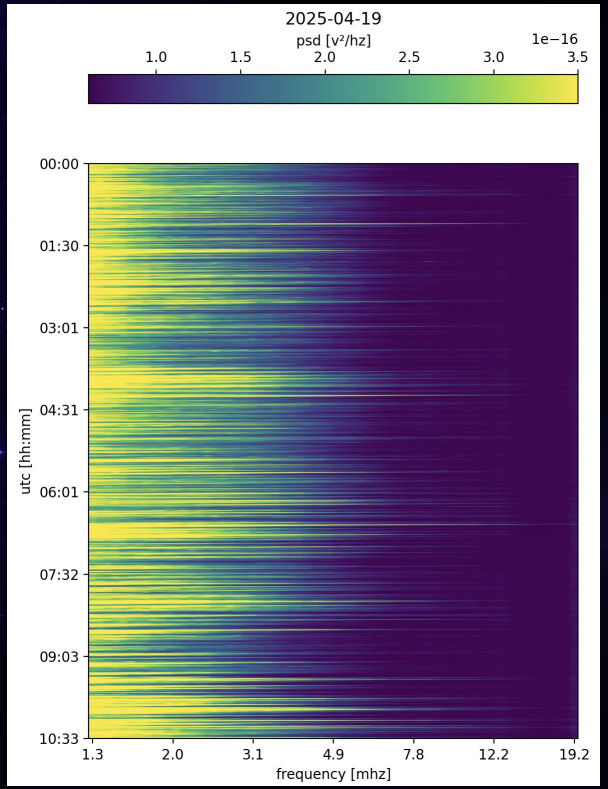

Methods

RFS HFR data is publicly available
Python packages used for data analysis:

- Numpy (array manipulation)
- Scipy (statistical analysis)
- Matplotlib (plotting imshow)
- Cdflib (data I/O)

Plots will be assessed to find solar radio bursts by observing PSD values and solar noise variation at different frequencies. And applying methods such as Stokes parameters to see where noise is strongest.

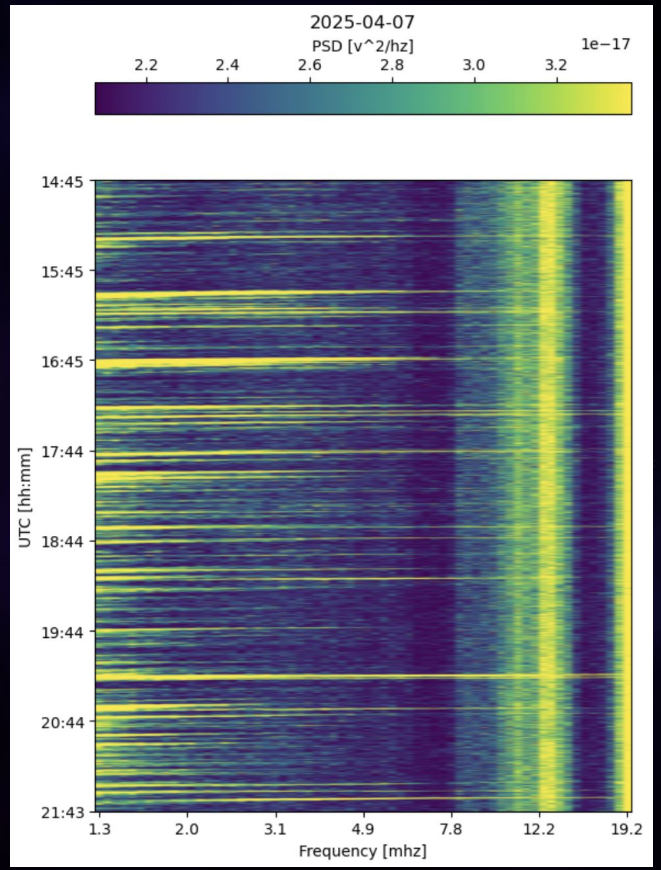

4 Budget/Resources

Budget/Resources

- PSP/FIELDS data is made public online by NASA
- Python (NumPy, SciPy, Matplotlib, CDFlib)
- As we will be using public data and online software, we are not expecting any expenses or the requirement of any physical equipment

5 Timeline

Goals from Late January to Mid April

Late Jan

Download data, set up shared repository, baseline loader and pcolormesh

Early Feb

Raw waterfall plots, time/freq formatting, check consistency for log-freq axis

Late Feb

Daily mean/STD spectra, identify quiet vs noisy intervals

Early - Mid March

Separate instrument noise from solar noise, compare filtered to raw data, solar-noise features

Late Mar - Early April

Summarize month-long trends, build combined plots, stacked spectra, daily noise timelines

Mid April

Finalize cleaned dataset and figures, prepare group presentation and poster

6 References

Bale, S.D., Goetz, K., Harvey, P.R., et al. (2016). The FIELDS Instrument Suite for Solar Probe Plus. Space Sci Rev 204, 49–82. https://doi.org/10.1007/s11214-016-0244-5

Kasper, J. C., et al. (2021). Parker Solar Probe Enters the Magnetically Dominated Solar Corona. *Physical Review Letters*, 127(25), 255101. https://doi.org/10.1103/PhysRevLett.127.255101

Mostafavi P., et al. (2024). Parker Solar Probe Observations of Collisional Effects on Thermalizing the Young Solar Wind. *Astronomy and Astrophysics*, 152. https://doi.org/10.1051/0004-6361/202347134

NASA. (2018). Parker Solar Probe: A Mission to Touch the Sun. *NASA Science*. https://www.nasa.gov/wp-content/uploads/2018/02/parkersolarprobe_presskit_august2018_final.pdf

Guo, Y. (2023). Flying Parker Solar Probe to touch the Sun. *Acta Astronautica, 214*, 110–124. https://doi.org/10.1016/j.actaastro.2023.10.020

Thank you!

Ajla/Soumay's Group

Rediscovery of the Higgs Boson with Bayesian Analysis

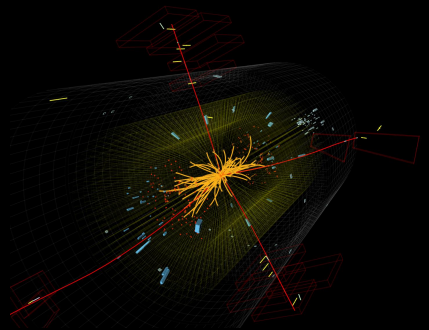

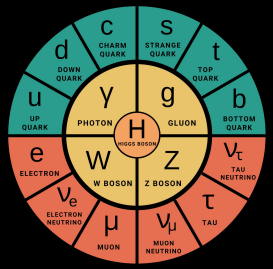

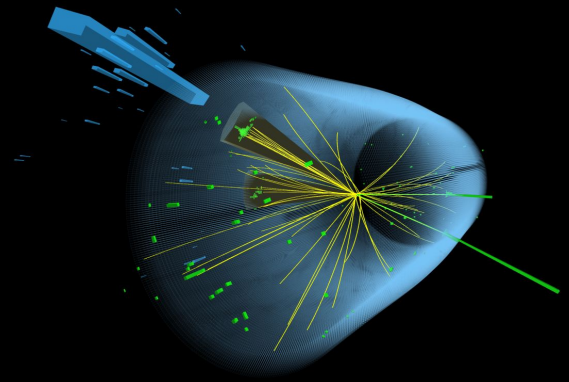

Mentors: Ajla Trumic & Soumay Garg

Mentees: Colton Abrahamson-Paradis, Audrey Clusin, Ryan Dalzell, Tarun Ganeshkumar, Emma Gaon, Ben Kyvik, & Anson Ng

Subject Background

Higgs Boson:

- The Standard Model
  - Fermions
    - Matter particles, half integer spin, obey Pauli Exclusion principle, quarks and leptons
  - Bosons
    - Force-carrying particles, integer spin
  - Higgs Boson
    - Give particles their mass, multiple decay modes

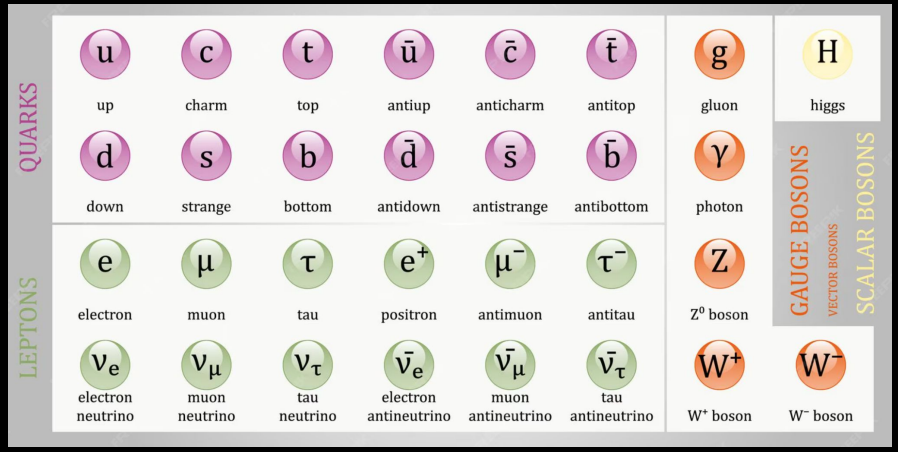

Table of Elementary Particles

Subject Background

Discovery:

- Experiment
  - Large Hadron Collider (LHC) at CERN
  - Proton-proton collision
  - Diphoton & W and Z boson decay channels
- Detector - ATLAS
  - Inner detector
  - Electromagnetic calorimeter
  - Muon spectrometer
- Frequentist analysis

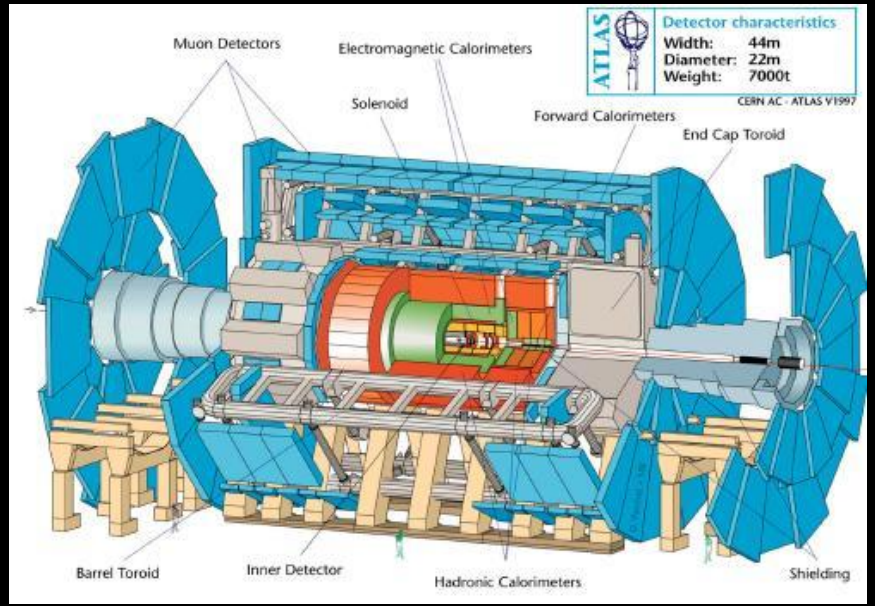

Subject Background

Bayesian Statistics:

- Statistical Inference: Frequentist vs. Bayesian
  - Long-run probabilities
  - Updating probability
- Bayes' Theorem
  - Priors - assumptions about parameters

Posterior → $$P(A_i|E) = \frac{P(E|A_i) \cdot P(A_i)}{\sum P(E|A_j) \cdot P(A_j)}$$

Subject Background

Parameters of Interest vs Nuisance Parameters:

- Interest: physical properties determined in experiment
  - Signal strength (μ = 1 = Higgs), Higgs Couplings, Higgs Mass and decay rate
- Nuisance: background parameters that clean data, help with uncertainty
  - Calibrations, detector accuracy, other systematic uncertainties
  - Bayesian analysis primarily used
  - Constrained via Probability Density Functions

Research Question

Project Goals:

- Rediscover (statistically) the Higgs boson
- Determine parameters of interest and nuisance parameter to fit the signal model
- Study the discovery sensitivity
- Comparison between frequentist and Bayesian analyses of the particle's invariant mass spectrum

Methodology

- **Step 1:** Data processing:
  - Retrieve Higgs datasets from CERN Open Data Portal
  - Data Cutting
    - Removing unusable data
  - Understanding detector effects
    - Process 1: Resolution Function
    - Process 2: Data Unfolding

$$P_{\text{obs}}(x) = \int_{-\infty}^{\infty} \left[P\left(x'\right) \cdot \epsilon(x') \right] R(x - x')\, dx'$$

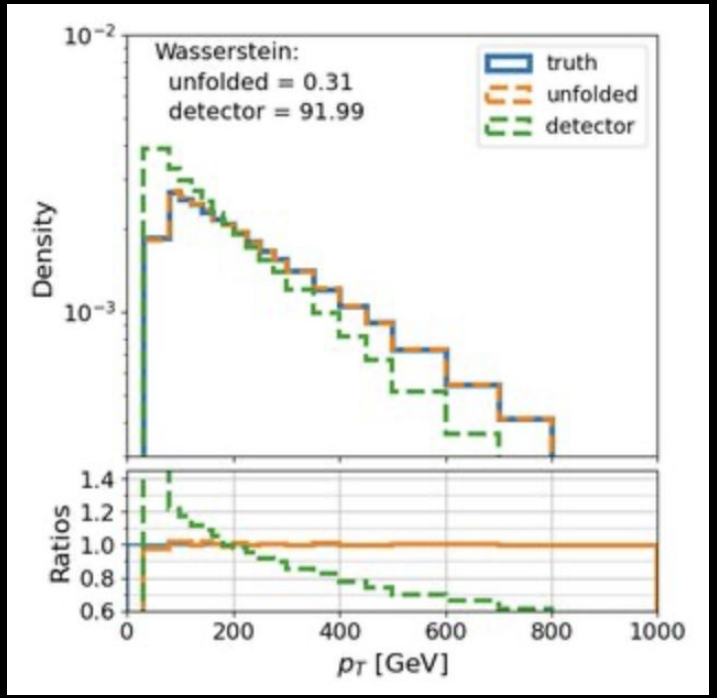

Towards Universal Unfolding of Detector Effects in High-Energy Physics using Denoising Diffusion Probabilistic Models (C.Pazos, 2024).

Methodology (continued)

- **Step 2:** Create Posterior Distribution
  - Estimate priors
    - Use theoretical spectrum, pre-Higgs search constraints to inform prior distributions
    - Set up reasonable parameter assumptions
  - Set up Poisson log-likelihood function
  - Compute posterior distribution from product of priors and likelihood function (Bayes Theorem)

Poisson log-likelihood function →

$$\ln \mathcal{L}(\theta) = \sum_{i=1}^{N_{\text{bins}}} \ln P(k_i \mid \lambda_i(\theta)) = \sum_{i=1}^{N_{\text{bins}}} \Big[k_i \ln(\lambda_i(\theta)) - \lambda_i(\theta) - \ln(k_i!) \Big]$$

Methodology (continued)

- **Step 3:** Posterior Sampling
  - Utilize Julia's BAT.jl Markov Chain Monte Carlo (MCMC) algorithms to optimize fit function
    - Metropolis-Hastings: Floats parameter to test effects on fit function (time intensive)
    - Hamiltonian Monte Carlo: Optimizes parameters based on Hamiltonian gradients (computationally intensive)
  - Determine optimal parameters, covariance matrices, and confidence intervals from MCMC
  - Learn about parameters of interest and nuisance parameters

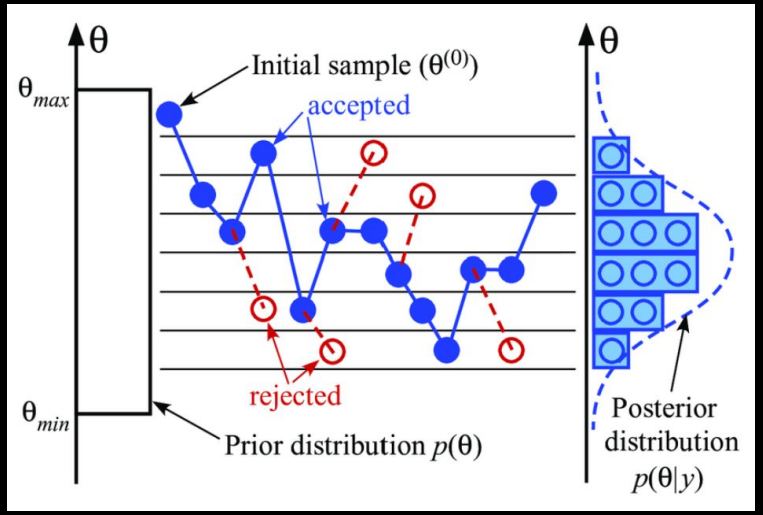

Methodology (continued)

- **Step 4:** Model Testing
  - Run toy experiments based on MCMC results
    - Generate Poisson fluctuated datasets similar to original ATLAS data
    - Plant Higgs signal within some toy distributions, leave others as “background-only”
    - Run toy distributions through our model to determine discovery sensitivity, set limits

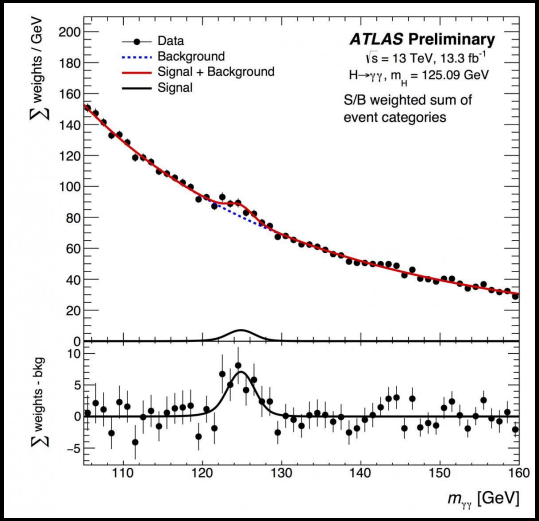

The distribution of the invariant mass of the two photons in the ATLAS measurement of H→γγ using the full 2015+2016 data set (ATLAS Experiment/CERN, 2016).

Methodology (continued)

- **Step 5:** Verify Results
  - Compare with ATLAS results
    - If Higgs discovery is replicated:
      - Analyze uncertainty
      - Improve model
    - If discrepancies found:
      - Re-fit and revise model
  - Analyze for new insights
    - Demonstrates potential for particle physics
      - Answers new questions

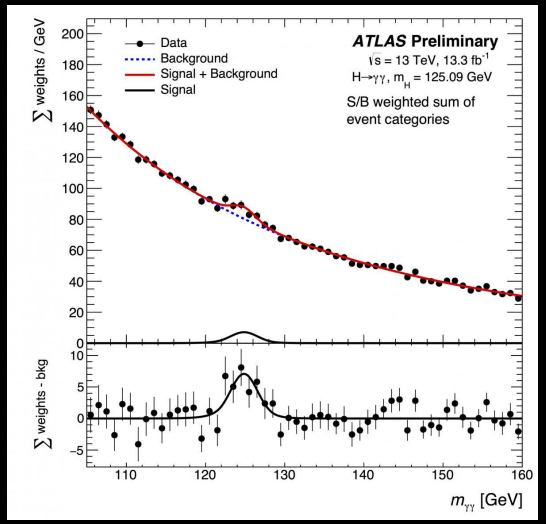

The distribution of the invariant mass of the two photons in the ATLAS measurement of H→γγ using the full 2015+2016 data set (ATLAS Experiment/CERN, 2016).

Budget & Resources

- Budget = Free!
- Higgs detection data from the CMS Open Data Portal
- BAT.jl package (Julia), Datahub
- Computational power–laptops

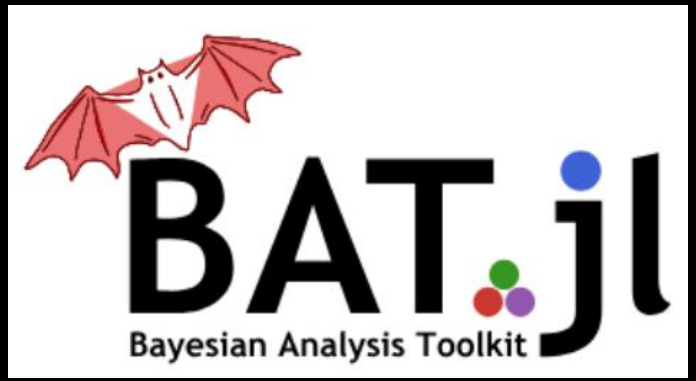

Project Timeline

12/20-1/19: Dataset Exploration and Technical Foundation

1/19-1/26: Detector-level Distribution Study

1/26-2/02: Resolution Function and Efficiency Modeling/Extraction

2/02-2/23: Forward Model/Unfolding Construction

2/23-3/02: Likelihood Function Construction

3/02-3/23: Posterior Sampling via MCMC and Debugging

3/23-3/30: Toy Dataset Generation and Evaluation of Discovery Sensitivity and Limits

3/30-4/13: Comparison with ATLAS/CMS results and Finalization

References

ATLAS Collaboration. (2012). Observation of a new particle in the search for the Standard Model Higgs boson with the ATLAS detector at the LHC. arXiv preprint. https://arxiv.org/pdf/1207.7214.pdf

ATLAS Collaboration. (2016). Atlas observes the higgs boson with run 2 data. ATLAS. https://atlas.cern/updates/briefing/atlas-observes-higgs-boson-run-2-data

ATLAS Collaboration. (2022). Measurements of the Higgs boson inclusive and differential fiducial cross-sections in the diphoton decay channel with pp collisions at √s = 13 tev with the ATLAS detector. arXiv preprint. https://arxiv.org/pdf/2202.00487.pdf

Fowlie, A. (2019). Bayesian and frequentist approaches to resonance searches. arXiv preprint. https://arxiv.org/pdf/1902.03243.pdf

Golchi, S., & Lockhart, R. (2016). A Bayesian search for the Higgs particle. arXiv preprint. https://arxiv.org/pdf/1501.02226.pdf

Golchi, S., & Lockhart, R. (2018). A frequency-calibrated Bayesian search for new particles. The Annals of Applied Statistics, 12 (3), 1939–1968. https://doi.org/10.1214/18-AOAS1138

Lista, L. (2023). Statistical methods for data analysis. Springer. https://doi.org/10.1007/978-3-031-19934-9

Pazos, C. (2024, June). (PDF) towards Universal Unfolding of detector effects in high-energy physics using denoising diffusion probabilistic models. Research Gate. https://www.researchgate.net/publication/381152936_Towards_Universal_Unfolding_of_Detector_Effects_in_High-Energy_Physics_using_Denoising_Diffusion_Probabilistic_Models

Tomic, Slavisa, et al. "Distributed localization with complemented RSS and AOA measurements: Theory and methods." Applied Sciences 10.1 (2019): 272.

Towards Universal Unfolding of Detector Effects in High-Energy Physics using Denoising Diffusion Probabilistic Models (C.Pazos, 2024).

Emmanuel’s Group

Quantifying EMIC-Plume Interactions as a Dominant Loss Mechanism for Electron Decay Rate in the Radiation Belts

Mentor: Emmanuel Paz
Mentees: Steven Su, Dashiell Rosberg, Emilian Sega

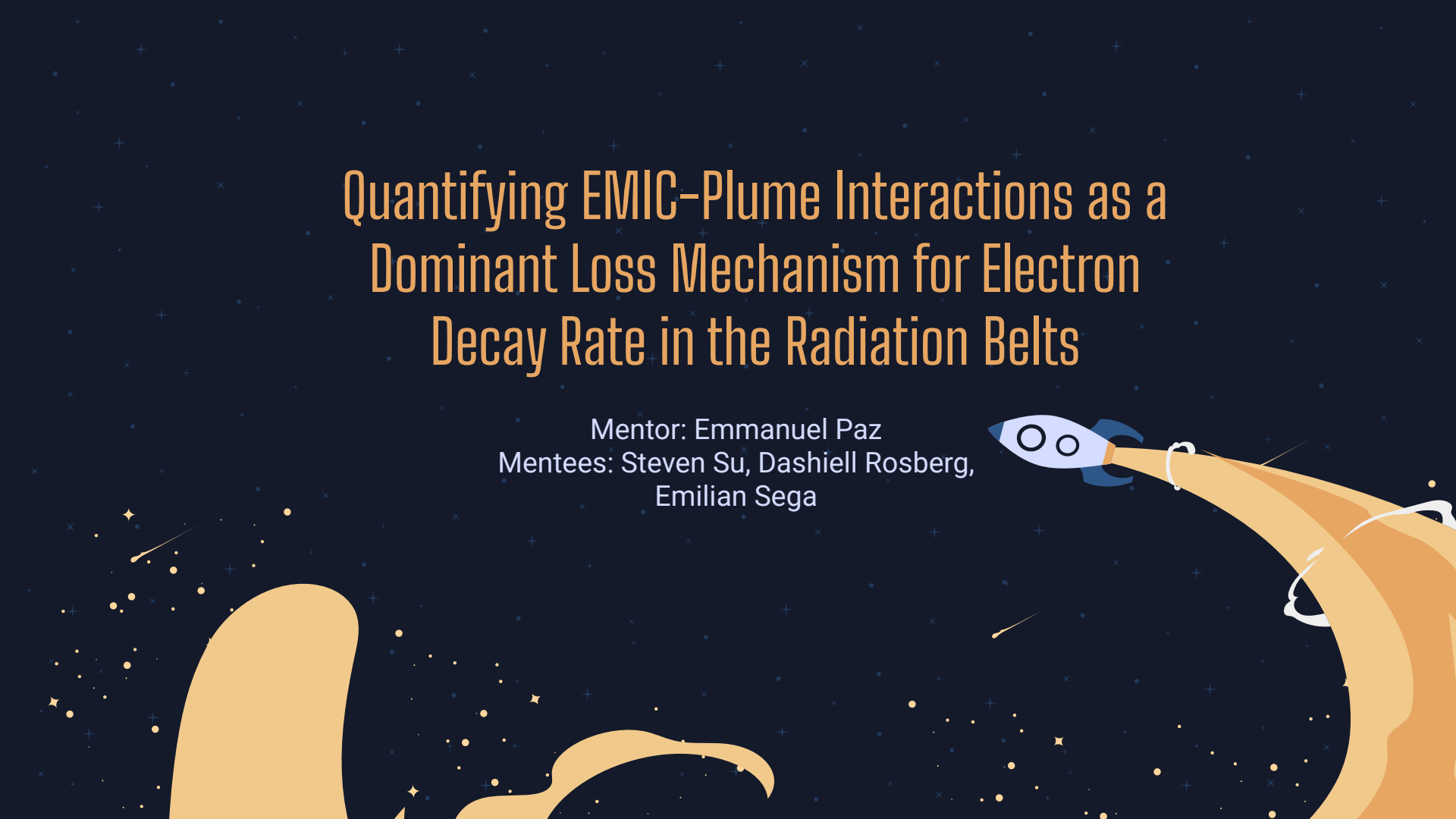

Contents

Plasmasphere & Radiation Belts

Plasmasphere

- Torus of cold, dense plasma
- 1-2 eV particles at 2-6 L-Shell
- Forms from ionospheric plasma travelling along magnetic field lines

Radiation Belts

→ Inner Belt:

- Protons (> 100 MeV) at 1.2–2.5 L-Shell

→ Outer Belt:

- Electrons (0.1–10 MeV) at 3–9 L-Shell (overlaps with outer radiation belt)
- Sensitive to geomagnetic conditions (Loss mechanisms: microbursts, radial diffusion, EMIC waves…)

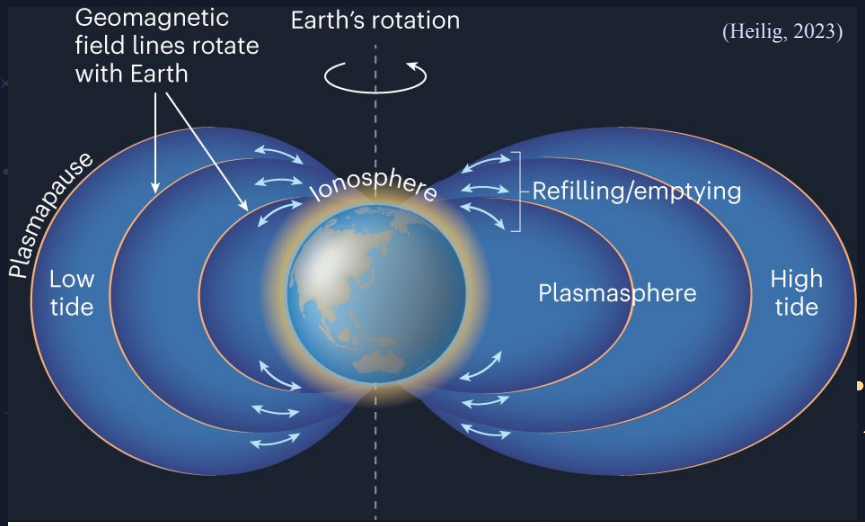

(Heilig, 2023)

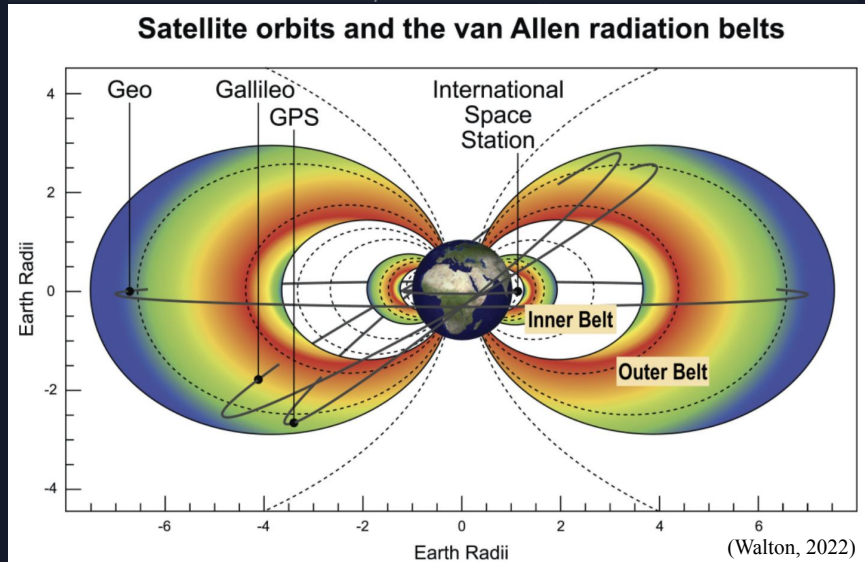

(Walton, 2022)

Background: Plasmaspheric Plumes

Corotation: the ExB drift driven by Earth's rotation that forces plasma to rotate around Earth at the same angular velocity as the planet.

Convection: the sun driven ExB drift produced by the solar wind generated dawn-to-dusk electric field that moves plasma sunward and causes erosion

The big idea: **competition**

- At lower L-shells, corotation dominates so plasma rotates around the Earth
- At higher L-shells, magnetic field strength decreases → convection drift dominates → plasma swept sunward → plume forms

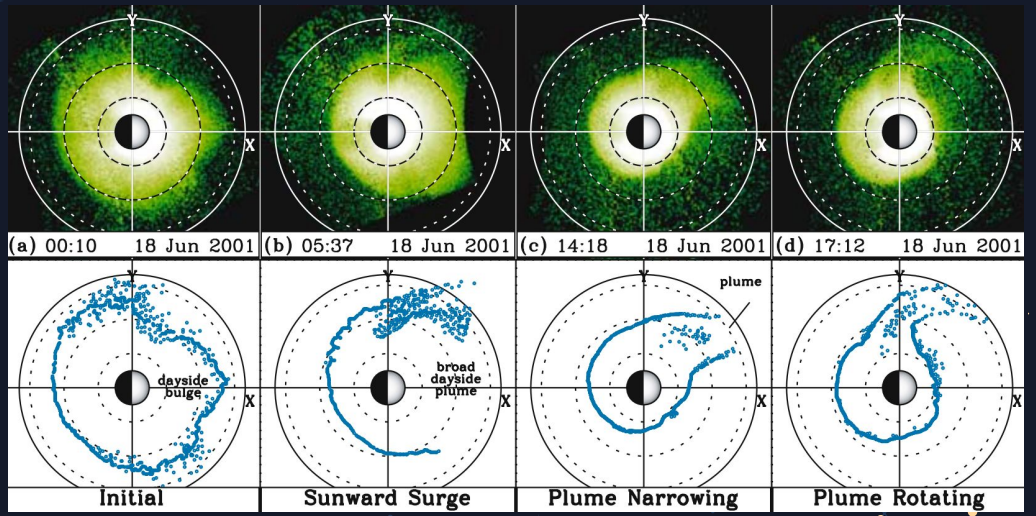

Background: EMIC (Electromagnetic Ion Cyclotron) waves

Origins:

- Tiny electromagnetic fluctuations (seed fluctuations) are always present in the plasma (thermal noise or background turbulence).
- Low-frequency plasma waves driven by temperature anisotropy ($T_\perp > T_{//}$) in ions (H^+, He^+, O^+). This free energy is transferred into these fluctuations to create EMIC waves via cyclotron resonance

Effects:

- Scatters electrons in the plasmasphere, increasing chances of precipitation/e^- decay

Interaction with Plumes:

- Plasmaspheric plumes enhance EMIC growth, acting as catalysts
- EMIC activity typically occurs at plume boundaries (since conditions favor ion resonance & wave growth)

Research Question

Different loss mechanisms affect different energy electrons:

- **Low** energy mechanisms (≤ 1 MeV): chorus and hiss waves, microbursts
- **High** energy mechanisms: EMIC waves, magnetopause shadowing, etc

To what extent are EMIC-plume interactions the dominant loss mechanism of higher energy electrons, and how does the agreement between the theoretical prediction from QLT and observed decay rates from the Van Allen Probes vary over different energy channels?

Our hypothesis: High energy electrons will have greater decay rates that match predictions from QLT, meaning EMICs are likely the dominant loss mechanism.

Methods: Identifying Plumes

PySpedas package (space & ground based data) → Van Allen Probes data

Criteria for identifying plumes:

(1) Van Allen Probes outside plasmapause (i.e. e^- density decreases by > 5x in 0.5 L shell)

(2) e^- density sharply increases (> 5x within 0.5 L shell), & exceeds that of Sheeley et al. (2001)'s model:

$$n_e = 1390 \, (3 / L)^{4.83} - 240 \, (3 / L)^{3.60}$$

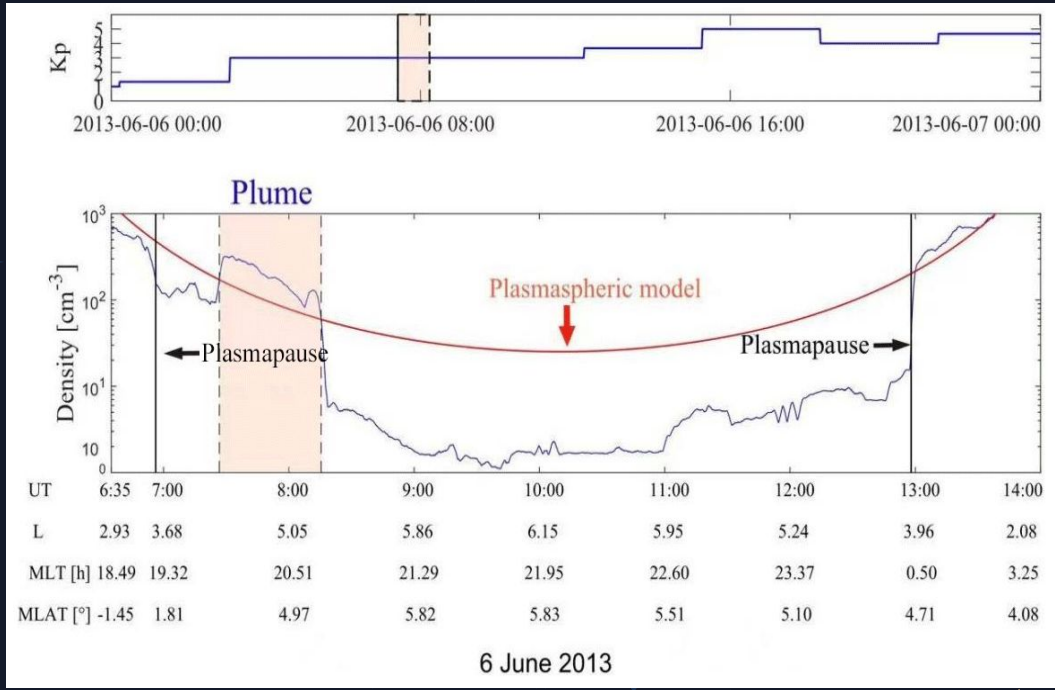

(Li et al., 2025)

Identifying EMIC Waves

EMIC waves resonate with 200 keV - 10 MeV

Plume-EMIC Events: Select events where EMIC waves and plumes occur together.

EMIC Wave Identification Methods

FFT: Analyze magnetic field (0–5 Hz) to get power spectral density (PSD).

Bands: Confirm EMIC in H^+, He^+, or O^+ gyrofrequency ranges.

Polarization: Left/Right test for verification.

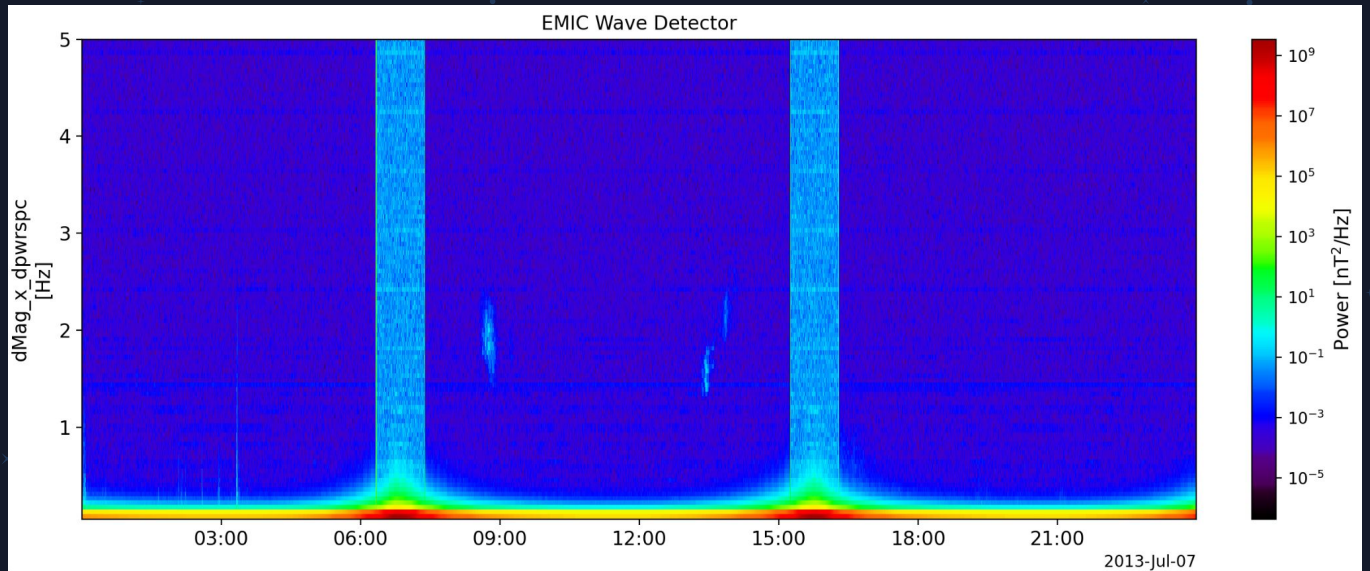

Obtaining the Observational Decay Rate / Lifetime (τ)

$$J(t) = J_0 e^{-t/\tau}$$

J_0 : initial e^- flux the moment e^- flux starts to decrease

J(t) : final e^- flux (immediately before flux begins to increase)

t : duration of the decreasing e^- flux

τ : decay rate/lifetime of e^- that remain trapped before scattering to atmosphere

Lifetime can be derived from the equation for all energy channels (ranges) on the satellite.

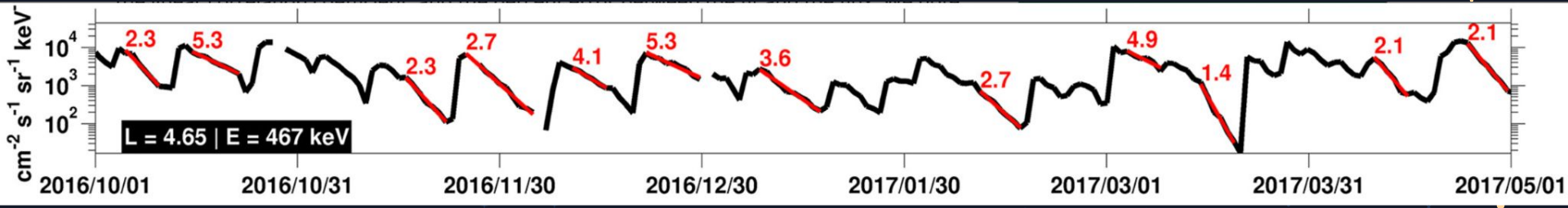

Using Quasi-linear Theory (QLT)

- QLT assumes weak and linear wave-particle interactions where the perturbation field is smaller than the background field
- Using the methods of Fast Fourier Transformations (FFT), we get inputs used for QLT: wave amplitude, density, B-field, ion composition, and wave-normal angle
- Using all these inputs, QLT calculates the pitch angle diffusion coefficient D_{aa} for EMIC scattering
- The theoretical lifetime is then obtained from the following equation

$$\tau_* \equiv \int_{\alpha_L}^{\frac{\pi}{2}} d\alpha \frac{cos\alpha}{2Dsin\alpha}$$

Timeline

1/29–2/16 Part 1: Find candidates of EMIC-Plume interacting events.

2/16–3/09 Part 2: Create a spectrogram showcasing the electron flux changing over time. Calculate the decay rate for all energy channels.

3/09–4/08 Part 3: Arguably the longest part of our project. Calculate the theoretical decay rate caused by the ”Super” EMIC wave using QLT.

4/13–4/20 Part 4: Compare the theoretical lifetime with the observed lifetime of electrons

References

Claudepierre, S. G., Ma, Q., Bortnik, J., O'Brien, T. P., Fennell, J. F., & Blake, J. B. (2020). Empirically Estimated Electron Lifetimes in the Earth's Radiation Belts: Van Allen Probe Observations. Geophysical Research Letters, 47(3). https://doi.org/10.1029/2019gl086053

Goldstein, J. (2005). Dynamic relationship between the outer radiation belt and the plasmapause during March–May 2001. *Geophysical Research Letters*, *32*(15). https://doi.org/10.1029/2005gl023431

Goldstein, J. (2006). Plasmasphere Response: Tutorial and Review of Recent Imaging Results. *Space Sciences Series of ISSI*, *124*, 203–216. https://doi.org/10.1007/978-0-387-69532-7_14

Heilig, B. (2023). Lunar modulations. *Nature Physics*, *19*(4), 467–468. https://doi.org/10.1038/s41567-022-01913-4

Li, H., Fu, T., Tang, R., Yuan, Z., Yang, Z., Ouyang, Z., & Deng, X. (2025). *Statistical study and corresponding evolution of plasmaspheric plumes under different levels of geomagnetic storms*. Copernicus.org. https://angeo.copernicus.org/articles/40/167/2022/angeo-40-167-2022-f01-web.png

Li, X., & Temerin, M. A. (2001). The Electron Radiation Belt. *Space Science Reviews*, *95*(1/2), 569–580. https://doi.org/10.1023/a:1005221108016

Ripoll, J. -F., Claudepierre, S. G., Ukhorskiy, A. Y., Colpitts, C., Li, X., Fennell, J. F., & Crabtree, C. (2020). Particle Dynamics in the Earth's Radiation Belts: Review of Current Research and Open Questions. *Journal of Geophysical Research: Space Physics*, *125*(5). https://doi.org/10.1029/2019ja026735

Selesnick, R. S., & Blake, J. B. (1997). Dynamics of the outer radiation belt. *Geophysical Research Letters*, *24*(11), 1347–1350. https://doi.org/10.1029/97gl51409

Walton, S. D. (2022, August 28). *The Evolution of the Electron Radiation Belt During Geomagnetic Storms*. ResearchGate. https://www.researchgate.net/publication/364591271_The_Evolution_of_the_Electron_Radiation_Belt_During_Geomagnetic_Storms

Yael’s Group

The Birth of CHAD

Lukas Beer, Jennifer Choi, Luke Engstrom, Benjamin Forsell, Nevin Green, Simon Nguyen

Background: The search for $0\nu\beta\beta$

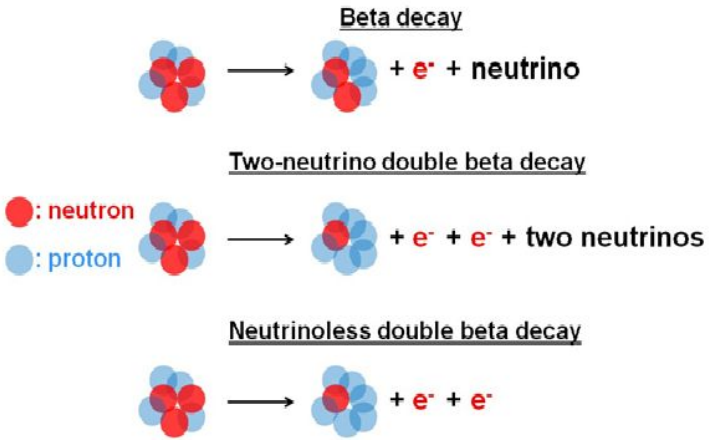

https://amore.ibs.re.kr/about/double-beta-decays/

Neutrinoless double-beta decay ($0\nu\beta\beta$):

- If no neutrinos escape/ only two electrons emitted:
  a. Emitted neutrino = absorbed neutrino
  b. Neutrino = own antiparticle (Majorana particle)

Significance:

- Violates lepton-number conservation → beyond the Standard Model.
- May explain matter–antimatter asymmetry.

Background: CUORE & CUPID

CUORE: 988 TeO_2 crystal bolometers at 10 mK
CUPID: added light detection for α/β discrimination
Berkeley Lab detector: 14 mK

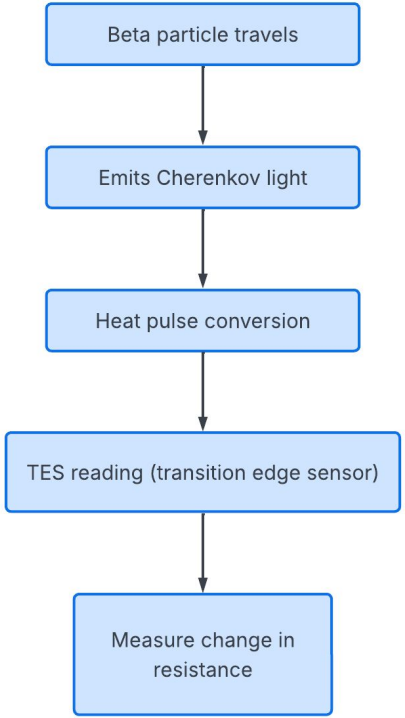

Background: Current Problem

- Signal output is extremely small
- Experiment must be extremely low noise
- mechanical vibrations
- Cryogenic temperature effects
- Energy resolution
- Background events

High Electron Mobility Transistors (HEMTS) offer a potential solution:
Low noise transistor, high speed, high performance at low temperatures

Research Question

Can we design a cryogenic HEMT-based charge amplifier low-noise, stable, and compact enough to be mounted close to a CUORE/CUPID bolometer that achieves competitive (or better) performance than existing JFET-based electronics?

Sub-Questions

1. What amplifier topology yields the lowest noise and most stable gain at cryogenic temperatures?

2. How should feedback, coupling, and biasing elements be sized for a T eO2 bolometer with ≈130 pF detector capacitance?

3. Can we create a manufacturable PCB that meets cryostat constraints for grounding, parasitics, and mechanical integration?

4. How close can we come to the ≈100 eVee baseline noise used by experiments such as CDMS and CUORE?

Methods

1. Choose HEMT (chose MGFC4419G HEMT transistor for voltage output properties)
2. Choose PCB design (based design off [1])
3. SPICE simulation for passive values
4. Create initial PCB layout
5. Order & solder
6. Test at cryostat testbed, 4k
    a. Measure signal, noise level, amplification
7. Revise layout accordingly & repeat testing until satisfactory results

Schematic & SPICE Simulation

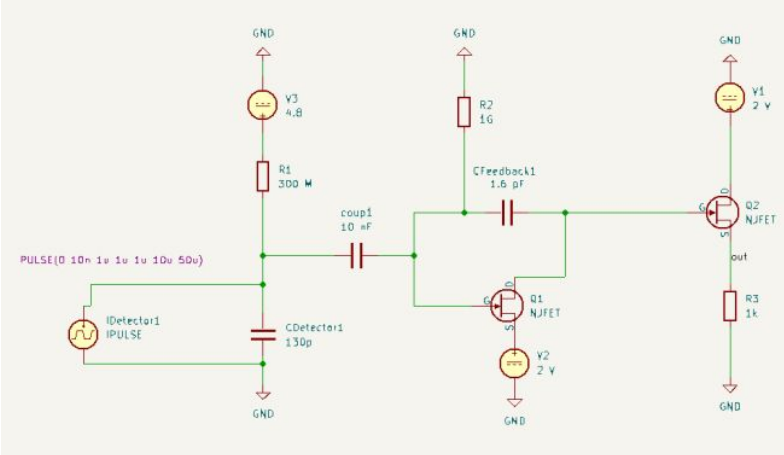

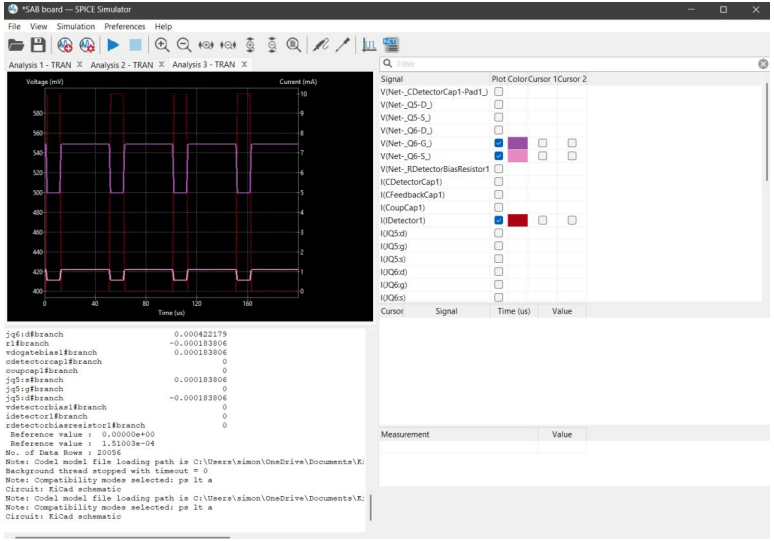

Layout

1. HEMT die is 0.3mm across and needs special equipment to be installed
2. Trace lengths must be reduced as much as possible
3. Board geometry should be formatted and designed for cryogenic temperatures

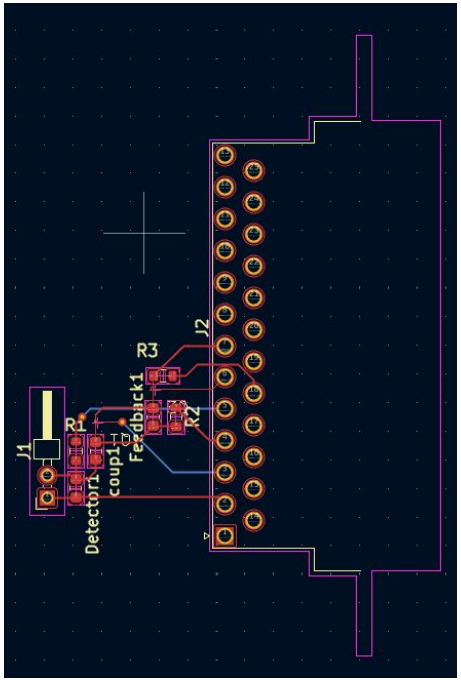

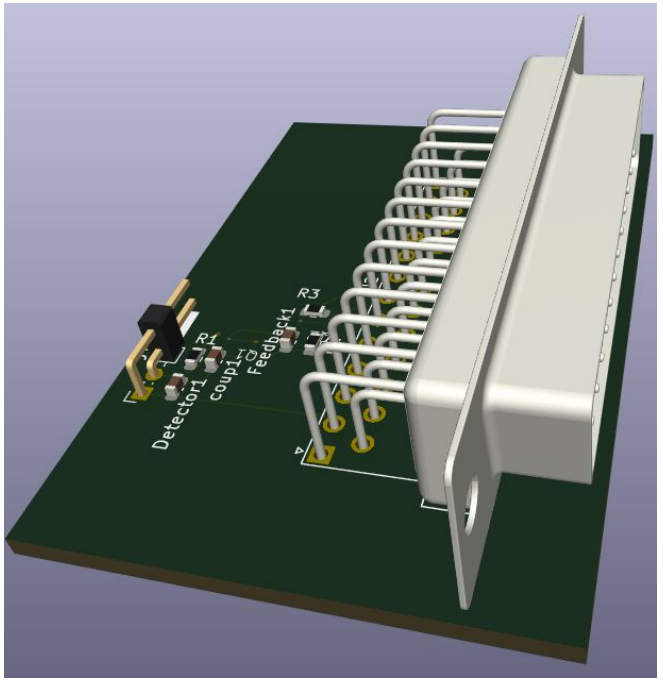

Budget/Resources

Budget ($400):

- PCB board - $200
- HEMT chips - $100
- Misc. PCB materials - $100

Resources:

- KiCad
- SPICE

Timeline

S1:
Weeks 1-3: theoretical study
Weeks 3-6: KiCad Schematic & PCB design
Weeks 6-10: Internal architecture comparison & refinement
Weeks 10-14: SPICE simulation
Weeks 14-15: Consolidation & mid-year report

S2:
Weeks 1-10: modify, assemble CHAD, order breadboard, test in room temperature, repeat
Week 11 (if possible): test final design in cryostat conditions
Week 12-14: buffer
Weeks 13-15: work on final deliverables

References

[1] A. Phipps, A. Juillard, B. Sadoulet, B. Serfass, and Y. Jin, "A HEMT-Based Cryogenic Charge Amplifier with sub-100 eVee Ionization Resolution for Massive Semiconductor Dark Matter Detectors," Nuclear Instruments and Methods in Physics Research Section A, 2019, arXiv:1611.09712.

[2] J. Anczarski et al., "Two-Stage Cryogenic HEMT-Based Amplifier for Low Temperature Detectors," arXiv:2311.02229, 2024.

[3] S. R. Chendvankar, "Charge Sensitive Preamplifier: Practical Notes for SERC School in Experimental High Energy Physics," Technical Note, Tata Institute of Fundamental Research.

[4] Mitsubishi Electric Corporation, "MGFC4419G InGaAs HEMT Chip Datasheet," Preliminary Specification, 1998.

[5] K. Lau, A. J. Steinbach, S. Chakram, et al., "Broadband Optical Modulation and Control at Millikelvin Temperatures," Nature, 2018.

[6] D. C. Moore et al., "Feasibility of a Fully Integrated HEMT-Based Charge Amplifier for Cryogenic Detectors," Review of Scientific Instruments, 2020.

[7] D. Phipps et al., "Low-Temperature Light Detectors: Neganov–Luke Amplification and Calibration," Journal of Low Temperature Physics, 2014.

[8] I. S. Shlimak, "Neutron Transmutation Doping in Semiconductors: Science and Applications," Physics of the Solid State, vol. 41, pp. 794–798, 1999.

[9] K. Schäffner et al., "Particle Discrimination in TeO2 Bolometers Using Light Detectors Read Out by Transition Edge Sensors," Astroparticle Physics, vol. 69, pp. 30–36, 2015.

[10] C. Ligi et al., "The CUORE Cryostat: A 1-ton Scale Setup for Bolometric Detectors," arXiv:1603.03306, 2016.

[11] Q. Dong, Y. X. Liang, D. Ferry, A. Cavanna, U. Gennser, L. Couraud, and Y. Jin, "Ultra-Low Noise High Electron Mobility Transistors for High-Impedance and Low-Frequency Deep Cryogenic Readout Electronics," Applied Physics Letters, vol. 105, 013504, 2014.